2.9 to 1.9 Ga paleoalterations ofArchean granitic basement of the Franceville basin (Gabon)

Idalina Moubiya Mouélé, Patrick Dudoignon, Abderrazak El Albani, Alain Meunier, Philippe Boulvais, François Gauthier-Lafaye, Jean-Louis Paquette, Hervé Martin, Michel Cuney

2.9 to 1.9 Ga paleoalterations ofArchean granitic basement of the Franceville basin (Gabon).

Idalina Moubiya Mouélé[a*], Patrick Dudoignon [a], Abderrazak El Albani [a], Alain Meunier [a], Philippe Boulvais[b], François Gauthier-Lafaye [c] Jean-Louis Paquette [def], Hervé Martin [def], Michel Cuney[g]

[a]UMR CNRS 7285, IC2MP, Bâtiment B35 – 5, avenue Albert Turpain, 86022 Poitiers cedex, France
[b]UMR 6118, département Géosciences, Université de Rennes, 35042 Rennes, France
[c]UMR 7517 CNRS, Laboratoire d'Hydrologie et de Géochimie de Strasbourg, 1 rue Blessig 67082, Strasbourg cedex, France
[d] Clermont Université, Université Blaise Pascal, Laboratoire Magmas et Volcans, BP 10448, F-63000 Clermont-Ferrand France
[e] CNRS, UMR 6524, LMV, F-63038 Clermont-Ferrand France
[f]IRD, R 163, LMV, F-63038 Clermont-Ferrand France
[g]GeoRessources UMR 7359, BP 239, F-54506 Vandoeuvre les Nancy

[*]Corresponding author.

Address: Paleocirculation and Diagenesis in Archean basement, Franceville basin, Gabon

Abstract

The Archean granitoids in the Kiéné area, Gabon, are overlained by the Paleoproterozoic sediments of the Franceville basin (2.1 Ga). The basin is known for its high-grade uranium deposits among which some have been forming natural nuclear fission reactors. Most of the studies were dedicated to the FA-FB Paleoproterozoic sediments hosting these uranium deposits. Little is known on the Archean basement itself and specifically on the hydrous alteration events it experienced before and after the sediment deposition. The present work is focused on their petrographical, mineralogical and geochemical characterization. Dating the successive alteration events has been attempted on altered monazite crystals.

Rocks in different alteration states have been sampled from eight drill cores crosscutting the Archean - Paleoproterozoic unconformity. The Archean granitoids observed in the deepest levels exhibit typical petrographical features of a propylitic alteration while they are intensely illitized up to the unconformity. The propylitic alteration is mainly pervasive but the original texture of the granitoïds is conserved in spite of the formation of new minerals: Mg-chlorite, allanite and epidote forming a typical paragenesis. The illitic alteration is much more invasive near the unconformity. The illitization process leads to the replacement of feldspars and the corrosion of quartz crysals by an illitic matrix while the ferromagnesian minerals are pseudomorphosed by a Fe-chlorite + phengite+ hematite assemblage. The final fluid-rock interaction step is marked by fissural deposits of calcite and anhydrite. The $\delta^{13}C$ isotopic data show that the fissural carbonates precipitated from diagenetic fluids enriched carbon products deriving from the maturation of organic matter. The U-Pb isotopic analyses performed on monazite crystals have dated three distinct events: 3.0-2.9 Ga (magmatic), 2.6 Ga (propylitic alteration) and 1.9 Ga (diagenetic illitization). The calculation of geochemical mass balances suggests that the water – rock ratio during the propylitic alteration event was weak. On the contrary, it was much higher during the overprinted illitization which is characterized by an intense leaching of Na, Ca, Mg, Sr, REE and an enrichment in K, Rb,Cs.

Neither the petrographic features nor the geochemical data militate for an Archean weathering event (paleosol). In the present case, diagenetic fluids have percolated from the unconformity into the basement where they overprinted the illitization processes upon the previously propylitized rocks. These fluids were probably oxidant as they are also responsible of the U mobilization which led to the formation of the ore deposits close to the FA-FB interface.

Keywords: Archean, granitoid, hydrothermal, Paleoproterozoic, diagenesis, Francevillian

Introduction

The Archean basements have been frequently altered by multiple hydrothermal and/or metamorphic events (Card, 1978; Murakami et al., 2011; Nedachi et al., 2005; Ohmoto, 1996; Ohmoto and Kerrick, 1977). Additionally, in some cases, their erosion surface may conserve the traces of weathering processes forming the so-called paleosols which are researched for their paleo-atmospheric signification (Grandstaff et al., 1986; Holland, 1994; Maynard, 1992; Mossman and Farrow, 1992; Ohmoto, 1996; Rye and Holland, 1998). At last, when overlain by sedimentary deposits, the basement rocks may have suffered mineral reactions triggered by the diagenetic fluid invasion (Mercadier et al., 2010). Because they are operating successively, all these events may superimpose their effects in some places. Then, the genetic message carried by the secondary minerals is difficult to interpret without an accurate petrographical study. This is the backbone of the present work whose goal is to characterize the alteration events which have affected the Archean basement under the Francevillian sedimentary series in Gabon. It was globally affected by post-magmatic to metamorphic mineral reactions (Mathieu, 1999; Sère, 1996) but its alteration state near the unconformity is still poorly documented. Our work, focused on that interface, was made possible thanks to several drill-holes which have been dug for uranium ore exploration. The goal is to determine the origin of the secondary minerals and to date their formation.

2. Geological setting

The Chaillu massif is located in the South Gabon which is Northeastern part of the Congo craton (Fig.1). It forms the granitic basement of the Paleoproterozoic sediments deposited in the Franceville basin. It is composed of different granitoid and orthogneiss bodies dated from 3.1 to 2.5 Ga (Bouton et al., 2009; Caen-Vachette et al., 1988). These bodies are structurally and mineralogically heterogeneous because of two major plutonic events (Bouton et al., 2009; Chevallier et al., 2002; Prian and Johan, 1989; Thiéblemont et al., 2009; Thomas et al., 2001). The first one took place during the Mesoarchean (2928 ± 6 Ma to 2870 ± 5 Ma). It led to the intrusion of gray-coloured calc-alkaline granitoids belonging to typical a Archean Trondhjemite, Tonalite, Granodiorite suite (TTG) associated with migmatized quartz diorites (Thiéblemont et al., 2009). Locally, these rocks are cross-cut by diorite sills. The second period of magmatism belongs to the Neoarchean (2800 to 2550 Ma). It is characterized by the intrusion of alkaline to calc-alkaline pink to red magmatic rocks: syenites, syenogranites, granites and pegmatites (Thiéblemont et al., 2009).

The Franceville basin sedimentary series are composed of five unmetamorphosed formations, 4000 m thick, sequentially labeled from FA at the base up to FE (Weber, 1968). The FA formation (500-1000 m thick) is directly deposited on the eroded surface of the Archean granitoids basement (Chaillu massif). It is essentially formed of conglomerates and sandstones typical of fluvio-deltaic deposits. Its upper part (Fig. 1) hosts the natural nuclear reactors of the Oklo, Okélobondo and Bangombé uranium ore bodies (Gauthier-Lafaye et al., 1996; Naudet, 1991). The FA formation in the Kiéné area, exhibits a vertical granulometric evolution (conglomerate to sandstone and mudstone). The color of the sediments changes upwards from red to green to black (Gauthier-Lafaye, 1986; Haubensack, 1981). The fine-grained black levels are

composed of detrital quartz, plagioclase and biotite. Plagioclase and biotite are locally replaced by calcite and illite + chlorite assemblage respectively (Haubensack, 1981). The green colored intermediate levels are rich in illite (or phengite) and chlorite which replace detrital biotite and locally feldspar. The sandstone is mainly composed of quartz grains cemented by calcite, illite and chlorite. The conglomeratic sandstones at the base of the FA sedimentary series lie directly on the granitoid basement. Their mineralogical composition is dominated by a microcrystalline illitic material filling the porosity and replacing feldspars. When disseminated between quartz crystals, the illitic matrix may contain calcite, anhydrite or gypsum. The sandstones at the very base of the series, are known to be red colored due to the precipitation of hematite in the cleavages of altered biotites and to the staining of detrital quartz grain surfaces. This is not the case in the eight studied drills crosscutting the unconformity we studied here: no trace of red coloration has been observed probably because detrital ferromagnesian minerals are lacking or perhaps, because of a secondary discoloration.

3. Sampling and analytical methods

3.1 Sampling

The eight drill cores studied here are located in the Kiéné region (250 km^2), the central part of the Franceville basin, close to the Mikouloungou U-ore deposit and the Kaya-Kaya fault (Fig. 2a). Petrographic investigations were performed on 38 samples collected along the eight drill cores (KA 13, GR1, GR5, GR23, GR31, GR20 GR43 and KA6) down to variable depth (5 to 36 m) below the unconformity between sandstones and granitic basement (Fig. 2b). From the deepest levels to the sediment interface, the granitoids exhibit three dominant “facies” which correspond to an increasing alteration degree: *(i)* the least altered one, observed at depth, are gray

TTG or pink-to-red syenitic-to-granitic rocks; *(ii)* the altered granitoids in which the initial petrographical texture is preserved; *(iii)* the intensely altered granitoids which are green colored close to the sandstone-basement unconformity for all the studied drill-cores. The granitoids are largely altered and red colored near the sandstone contact in the GR20 and GR31 drill cores (Fig. 2b).

3.2 Analytical methods

The petrographical observations of the granitoids were performed using optical and scanning electron microscopes (OM, SEM). Polished thin sections were carbon coated before examination using the backscattered electron mode imaging (Jeol JSM 5600LV). X-ray spectra were collected with an energy dispersive device according to following analytical conditions: 15 kV accelerating voltage, 1 nA probe current and a 16.5 mm focalization distance. Micro-chemical analyses were obtained using a CAMECA SX50 electron microprobe (CAMPARIS analytical center, University Pierre and Marie Curie, Paris VI) equipped with wavelength dispersive spectrometers (15 kV accelerating voltage, 1 nA probe current, 1µm beam spot diameter). Bulk rock analyses were carried out at the SARM-CRPG (Nancy, France; Table 1). The samples were fused with $LiBO_2$, dissolved with HNO_3, analyzed using ICP-EAS and ICP-MS for major and trace elements respectively. The calibration is based on international standards. The mineralogical composition of each sample has been determined using X-ray diffraction of randomly oriented powders (Bruker D8 ADVANCE A25 diffractometer, CuKα). The accelerating voltage and probe current were of 40KV and 40 mA, respectively. Clay mineral identification was detailed using oriented < 2µm preparations scanned in the air dried and ethylene glycol saturation states in the 8 to 30° 2θ CuKα angular range. The C and O isotope compositions of calcitic veins were measured in the stable isotope laboratory of the Géosciences department (Rennes, University of Rennes 1).

Calcite was reacted with anhydrous H_3PO_4 at 50°C and the isotopic compositions measured on a triple collector VG Optima mass spectrometer.

The monazite crystals observed in two samples (KA6 437.85 and GR1 631) near the unconformity level were used to constrain the ages of plutonic rock emplacement and their subsequent alterations. These crystals were examined using SEM, mostly in backscattered electron mode, and analyzed using a CAMECA SX50 electron microprobe (CAMPARIS center, University Pierre and Marie Curie, Paris VI). U-Th-Pb isotopic data were obtained by laser ablation inductively coupled plasma spectrometry (LA-ICPMS) at the Volcanology Laboratory of Clermont-Ferrand University. The analyses involved the ablation of minerals using a Resonetics Resolution M-50 powered by an ultra-short-pulse (<4ns) ATL Atlex Excimer laser system operating at a wavelength of 193 nm (Muller et al., 2009). A 7 µm laser spot diameter and repetition rate of 1 Hz with energy of 8 mJ producing a fluence of 15 J/cm^2 was used for zircon dating. The ablated material was carried into helium flux and then mixed with nitrogen and argon before injection into the plasma source of an Agilent 7500 cs ICP-MS equipped with a dual pumping system to enhance the sensitivity. The alignment of the instrument and mass calibration were performed before each analytical session using the NIST SRM 612 reference glass, by inspecting the signal of ^{238}U and by minimising the ThO^+/Th^+ ratio (< 1%).The mean sensitivity for ^{238}U using a spot size of 44 µm is about 25,000 cps/ppm. The analytical method for isotope dating of zircon with laser ablation ICPMS is similar to that developed for monazite and reported by Paquette and Tiepolo (2007). The signals of ^{204}(Pb+Hg), ^{206}Pb, ^{207}Pb, ^{208}Pb, ^{232}Th and ^{238}U masses are acquired. The occurrence of common Pb in the sample can be monitored by the evolution of the ^{204}(Pb+Hg) signal intensity, but no common Pb correction was applied owing to the large isobaric interference from Hg. The ^{235}U signal is calculated from ^{238}U on the basis of the

ratio $^{238}U/^{235}U$= 137.88. The analyse procedure is based on 30 seconds of background integration with laser off followed by 1 minute integration with the laser firing and a 30 seconds delay to wash out the previous sample and prepare the next analysis. Data are corrected for U-Pb fractionation occurring during laser sampling and for instrumental mass discrimination (mass bias) by standard bracketing with repeated measurements of the Moacyr monazite standard (Gasquet et al., 2010). Repeated analyses of Manangoutry monazite standard (Paquette and Tiepolo, 2007), treated as unknown, independently control the reproducibility and accuracy of the corrections. Data reduction was carried out with the software package GLITTER® from Macquarie Research Ltd (Achterbergh et al., 2001; Jackson et al., 2004). For each analysis, the time resolved signal of single isotopes and isotope ratios was monitored and carefully inspected to check the presence of perturbations related to inclusions, fractures, mixing of different age domains or common Pb. Calculated ratios were exported and Concordia $^{206}Pb/^{238}U$ vs $^{208}Pb/^{232}Th$ ages and diagrams were generated using the Isoplot/Ex v. 3.23 software package (Ludwig, 2001).The concentrations in U-Th-Pb were calibrated relative to the certified contents of Moacyr monazite standard (Seydoux-Guillaume et al., 2002).

4. Results

4.1. The least-altered granitoids

The least altered gray or pink-to-red granitoids are observed in the deepest parts of the different drill cores far from the unconformity (Fig. 2b). The primary minerals are quartz, plagioclase (An_0 –An_{20}), biotite, alkali feldspar and locally amphibole. Zircon, apatite, uranothorite and monazite are the common accessory mineral phases. The gray granitoids present sometimes a gneissic structure.

The magmatic rocks range from diorite to granite. The whole rock major element compositions of the less altered rocks reflect the variety of these rock types (Table 1): i.e. SiO_2 (52.1 - 74.5 wt%), FeO_T (0.3 - 9.5 wt%), MgO (0.16 - 6.7 wt%). In order to determine their magmatic type, the chemical composition of these rocks has been plotted in the Q-P chemical-mineralogical diagram of Debon and Le fort (1983) (Fig.3). Because even the best preserved samples from the eight drill cores exhibit petrographic features of a hydrothermal alteration event the rock samples were selected according to their low ignition loss value: 2.5 Wt%. The grey TTGs range from quartz-diorite (dq) to tonalite (to) composition, while the pink and red rocks correspond to granodiorite (gd) and adamellite (ad) (Table 1; Fig. 3). The chondrite-normalized REE patterns show that tonalities present the typical highly fractionated pattern: high LREE content, low HREE content, no significant Eu anomaly. These properties are typical of the Archean TTG (Martin, 1986). On the other hand, the granodiorite and adamellite have lower REE contents with a positive Eu anomaly; such REE patterns have already been interpreted in Archean rocks as resulting from the fractionation by accessory phases such as allanite and zircon (Martin, 1987)(Fig. 4). Finally the higher REE content of the diorite is similar to that of the late Archean sanukitoids (Martin et al., 2010; Stern, 1989). In other words, all the less altered rock samples display the features typical of late Archean magmatic associations.

4.2. The altered granitoids

4.2.1. Samples located far from the unconformity

All the Kiéné granitoid samples located far from the unconformity exhibit the presence of chlorite. A pervasive chloritization process has severely affected the primary ferromagnesian minerals, i.e. total replacement of biotite and amphibole. Chlorite is associated to epidote, titanite

and allanite (Fig. 5a). According to Lowell and Guilbert, (1970) and Titley et al. (1986), this paragenesis is typical of a propylitic alteration. Concomitantly, the plagioclases are partially replaced by small sized micas (sericite) forming a microcrystalline matrix in which calcite, pyrite and chalcopyrite crystals are locally disseminated. Some fractures crosscut the propylitzed rocks. They are filled by a zoned deposit: chlorite along the walls and calcite sealing the central part (fig. 5b)

4.2.2. Samples close to the unconformity

The Kiéné granitoids are affected by an intense illitization in the vicinity of unconformity giving them a green color. This alteration is mainly invasive and extends down to 4-5 m depth. Plagioclase, K-feldspar and previously chloritized biotite are totally or partially replaced by illite (Fig.6a and b). The feldspars are corroded by a microcrystalline matrix (5-20 µm) while the chloritized biotite are replaced by larger illite crystals (10-50µm). The quartz bodies, themselves, exhibit corrosion features and are locally crosscut by illite veinlets. The illitization intensity decreases with depth becoming nearly undetectable between 5 and 7 m down from the unconformity. Here, only illite veinlets are still observable. Close to the unconformity, the GR20, GR23 and GR31 granitoid samples become red colored. The chloritized biotites are replaced by an illite + hematite assemblage (Fig. 6b). The rocks are crosscut by calcite ± anhydrite veins (Fig. 6c). Some monazites have been locally observed disseminated through the illitic matrix.

4.2.3. Alteration features of FA sandstones

The FA sandstones above the unconformity exhibit detrital quartz and K-feldspar crystals embedded in an illitic micro-crystalline matrix while the detrital grains, whatever their composition, are invaded along their inter-granular joints. Samples GR23 629 and GR20 818 are cemented by anhydrite and/or calcite deposits (Fig. 6d).

4.3. Geochemical data of bulk rocks

Because of the predominance of hydrolyzed and carbonated secondary phases in the secondary minerals, the loss on ignition (L.O.I) has been chosen here as an indicator of the alteration degree. In most samples, L.O.I. is significantly greater than that of the corresponding unaltered rocks. Indeed, the measured values range from 0.76 wt% in the freshest granitoids to 4.5 wt% for the most altered. However, the average L.O.I. calculated from a compilation of 60 TTG samples, is much lower: 0.25 wt% (Huang et al., 2013). Consequently, the absolute value of L.O.I. cannot be directly used as a reliable marker because of two reasons: (i) for a given rock type, it depends on the quantity of secondary minerals produced by alteration processes; (ii) it varies according to rock types. For instance, diorite L.O.I. typically averages to 1.55 wt% (Debon and Le Fort, 1983), tonalite for 0.32 and granodiorite for 0.12 (Huang et al., 2013). The tonalite value will be used here as the reference in the calculation of relative L.O.I. variations $\Delta LOI = (LOI_{sample} - LOI_{ref})/(LOI_{most\ altered\ sample} - LOI_{ref})$. According to this definition, the ΔLOI calculated for each basement sample shows a regular increase toward the unconformity (Fig. 9). The most altered levels are found in the illitic zone in agreement with petrographic observations. In order to address the problem of element mobility, it appears suitable to normalize all chemical element values to that one remaining immobile during the alteration processes. As already proposed by

several authors (Nesbitt, 1979; Ohmoto, 1996; Rye and Holland, 1998; White et al., 2001), Ti or Zr are classically considered as reference immobile elements. Here, Ti has been chosen because of its higher content. Then, each element content in the altered samples is corrected by the $TiO_{2\ reference}/TiO_{2\ sample}$ ratio. Propylitic and illitic processes being acceptably discriminated by the increasing loss on ignition (Fig. 7), the ΔLOI parameter has been used to study the variations of the major and some minor element amounts as a function of alteration intensity (Figs. 8 and 9). These variations between altered and reference samples (defined by the lowest ΔLOI) are calculated as follows: $\Delta SiO_{2sample} = (SiO_{2\ sample} \times TiO_{2\ reference}/TiO_{2\ sample}) - SiO_{2\ reference}$ (wt%). Because the piece of rocks sampled in the drill cores cannot be at the size of a representative sample, the experimental error is not calculable. This is why we adapted the variation scales to their abundance in the specimens: 0 to 50 for SiO_2 and Al_2O_3, -7 to 2 for all the other components. Reported in the same scale, ΔSiO_2 and ΔAl_2O_3 show contrasted distribution with ΔLOI: the first one is systematically negative while the second remains roughly constant. Silica loss and aluminium conservation are commonly reported in water rock interactions due to their large difference of solubility. The weight percent variations are more limited for Fe_2O_3, MgO and CaO. If they are not significant for the first and second ones, it seems that the losses of the calcium are more important in the illitic alteration zone. The chemical differences between propylitized and illitized samples are clearly evidenced by the alkaline element behaviour. All exhibit increasing losses of Na_2O with ΔLOI but they more important for the second ones. The K_2O amount remains roughly constant in the propylitized zone while it significantly increases in the illitic one. The variations for trace elements are expressed in ppm (Fig. 9). The illitized samples are enriched in rubidium and cesium because of their potassium similar chemical affinities for micas. Strontium is depleted in all the samples, the losses being more important in

the illitized ones. Cerium and lanthanium amounts are highly variable in the propylitized samples while they are systematically depleted in the illitized ones (Figs. 9 and 10). The variations of uranium are erratic but thorium seems to be systematically depleted. In spite of the uncertainties due to the limited size of the samples, it is possible to distinguish the geochemical characteristics of the two alteration types. Indeed, the propylitic alteration is almost chemically conservative: the losses of SiO_2 and Na_2O are limited. This is not the case for illitization which is depleted in all the components except aluminium (conserved) and potassium (enriched). The behaviour of trace elements outlines this difference.

4.4. Crystallo-chemistry of secondary phases

Chlorite and illite-phengite are present in all the studied samples. It is to be noticed that no di- or trioctahedral expandable mixed-layer minerals have been detected in the studied samples (Fig. 11a).

4.4.1. Chlorite

XRD patterns of randomly oriented powders show that chlorites are of the IIb polytype. The (001)/(002) peak intensity ratio decreases from depth to top (0.60-0.50 to 0.20) indicating that the relative proportion of Fe and Mg ions changes from the deep propylitic zone to the upper illitic level (Fig. 11b). This is coherent with the micro-chemical analyses of individual chlorite crystals. Most of the half-formula units calculated on a 14 oxygen basis, plot inside the brunsvigite composition field defined by Foster (1960). This is the case for all the chlorites in the propylitic zone (Table 2, Table 3, Fig. 12b). The Fe/(Fe+Mg) ratio varies from 0.3-0.5 (propylitic zone) to 0.6 – 0.7 (illitic level).

4.4.2. Illite-phengite

The XRD patterns of randomly oriented powders indicate that the illite-phengite minerals are composed of a mixture of $2M_1$ and 1M polytypes. They are small sized crystals when replacing the feldspars or infilling the quartz microcracks (5-20µm) but become larger when replacing chlorites (10-50µm). Their half-formula units calculated from microprobe analyses using a 11 oxygen basis, are coherent with that of dioctahedral micaceous minerals (Tables 4, 5). Two populations are clearly separated in the MR^{3+}, $2R^{3+}$, $3R^{2+}$ diagram proposed by Velde (1985).The phengitic crystals are found in the altered chlorites as shown by the mixing line while the illitic ones are found in the altered feldspars (Fig. 12a). Both exhibit a quite similar range of Fe/(Fe+Mg) ratio: 0.46-0.61 and to 0.52-0.76 for phengite and illite respectively. However, phengites are always K-richer than illite: 0.84-0.95 and 0.73-0.84 respectively.

4.4.3. Epidote-allanite

Epidotes are of the pistachite type (Table 6). They form everywhere in the rock, partly replacing primary feldspars or chloritized biotites or precipitating into veinlets. Their Fe/(Fe+Al) ratio varies from 0.30 to 0.42. Allanite crystals, on the contrary, form exclusively in chloritized biotites. They present a rather constant Fe/(Fe+Al) ratio (0.3-0.32). Their main chemical characteristic is the very high Nd, Ce and La contents: 0.16-0.07, 0.38-0.36, 0.25-0.17%respectively.

4.4.4. Monazite

Monazite crystals have been observed in two samples: KA6 437.85 (0.85 m from the unconformity) and GR1 631 (1 m from unconformity). The first one is a strongly illitized rock containing Fe-rich chlorites. Euhedral elongated millimeter size crystals of monazite are scattered in the illitic matrix. They seem to be perfectly unaltered and do not exhibit any chemical zoning

in spite of light grey intensity variations observed in the BSE imaging contrast (Table 7). The GR1 631 sample is less illitized since only feldspars are altered. Most of the micro-cracks are filled by calcite, and locally by quartz and pyrite**.** Here, the monazite crystals are anhedral, often grouped in aggregates and intimately associated with sulfide and illite. Compared to the euhedral crystals of the KA6 437.85 sample, monazite crystals of the GR1 631 one exhibit higher U, La and Ce and lower Th, Ca, Nd, Sm contents. The Th/U ratios are very low (Tables 8.9). They are characterized by lower Th content (Th<12000 ppm) compared to that of the unaltered monazites described by Mathieu et al. (2001) in the FA Sandstone (average Th = 40000 ppm for 94 analyses).

4.4.5. Carbonates

Calcite is observed in many samples from depth to the upper levels in the FA sandstone. Far from the unconformity in the propylitic zone, it appears as xenormorphic crystals located in altered plagioclase and in veinlets where it is associated to chlorite. It is observed as euhedral crystals filling the fissures near the unconformity where it is locally associated to anhydrite. In some of the FA sandstone samples, it constitutes the inter-granular microcrystalline cement. Regardless of their habit, the calcite crystals do not show significant chemical composition differences.

4.5. Geochronological data

The isotopic dating using laser-ICPMS microanalyses were performed on monazite crystals sampled near the FA sandstone-granitoid unconformity in the KA6 437.85 and GR1631 (Tables 8 and 9). The first one is Th-rich (11614-2909 ppm). Plotted in the $^{206}Pb/^{238}U$ versus $^{207}Pb/^{235}U$ diagram (Fig. 13), the U-Pb data of the KA6 437.85 monazite give two groups of discordia ages:

295 from 2998±25Ma (MSWD = 0.72) to 2922±24 Ma (MSWD = 1.4) and 2621±30Ma (MSWD =
296 1.5). The GR1 631 monazite being common Pb-rich, the dating is obtained using the $^{207}Pb/^{206}Pb$
297 versus $^{206}Pb/^{238}U$. The Tera-Wasserburg diagram (Fig. 14) gives an age of 1870 ± 26Ma (MSWD
298 = 1.04).

299

300 **4.6. C and O isotope compositions of calcite**

301 The calcite isotopic analyses were performed on the propylitized and illitized granitoids far
302 from and closed to the unconformity respectively. The $\delta^{13}C$ values obtained varies from -5 to -
303 14‰ and the $\delta^{18}O$ ones from 10.2 and 17.7‰, most of them being close to 10.5 – 11‰ (Tab. 10).
304 The C and O isotope compositions are not inter-correlated, nor with depth, intensity of
305 carbonation, nature of alteration (propylitization, illitization), or element mobility.

306 The large range of $\delta^{13}C$ values suggest that carbon comes from two different sources: one
307 having a $\delta^{13}C > -5$‰, which might be surface-derived continental carbon including atmospheric
308 CO_2, and another one having a $\delta^{13}C < -14$‰, which could possibly be a signature of the evolved
309 organic matter similar to that identified in the sediments of the Franceville Basin (Albani et al.,
310 2010; Weber and Gauthier-Lafaye, 2013). The $\delta^{18}O$ values centered around 10.5 – 11‰ point to
311 formation at low temperature hydrothermal conditions (150-300°C), which is consistent with the
312 common mineralogical association of calcite + chlorite, where the fluids reached isotopic
313 equilibrium with the granitic basement. On the other hand, the KA6462 sample has a much
314 higher $\delta^{18}O$ value, which probably relates to calcite formation at lower temperatures than for the
315 others, regardless of the nature of the fluid involved in calcite crystallization.

As a whole, the C and O isotope compositions are consistent with the presence of a diagenetic fluid that would have circulated along or close to the unconformity, imposing low temperature hydrothermal conditions to secondary alteration processes as it is the case for the Athabasca basin (Richard et al., 2013). Part of the carbon was taken from the organic matter which is particularly abundant in the FB Francevillian sediments. A similar case is given by the Athabasca basin where metamorphic fluids have interacted with graphite bearing metasediments of the basement. These fluids have been able to precipitate calcite with such isotopic signatures, at greenschists conditions, in equilibrium with chlorite.

5. Discussion

5.1. Propylitic alteration

Sère (1996) interpreted the presence of chlorite, albite, quartz and calcite in veins crosscutting the Chaillu massif as witnessing a metamorphic episode of the greenschist facies type. The petrographic observation performed on the eight drill cores show that all the biotite crystals have been chloritized regardless of the parent rock type: granitoids or gneiss. This implies that the chloritization took place after deformation. Consequently, it cannot be related to a metamorphic event but rather to a propylitic alteration which preserves the texture of rocks. Indeed, the chlorite-sericite-epidote/calcite assemblage is commonly described in propylitized granitoids (Lowell and Guilbert, 1970; Titley et al., 1986).

The $\Delta Fe_2O_3/TiO_2$, $\Delta MgO/TiO_2$, $\Delta CaO/TiO_2$, and $\Delta K_2O/TiO_2$ ratios do not vary with ΔLOI in the propylitic zone (Fig 10). Some samples plot far from general trend due to the local invasion by secondary minerals such as calcite (high CaO/TiO_2 ratio-GR23 631) in fracture and plagioclase. The $\Delta SiO_2/TiO_2$ and $\Delta Na_2O/TiO_2$ ratios decrease slightly while $\Delta Al_2O_3/TiO_2$ remains roughly

constant. This means that the propylitized rocks do not have experienced significant exchanges of chemical component with the external reservoir. It is a nearly isochemical set of mineral reactions in which the potassium released by biotite during chloritization is consumed by the crystallization of sericite. This is typical of propylitic alteration in which the water/rock ratio is limited (Berger and Velde, 1992). The temperature conditions can be roughly estimated using mineral indicators. The allanite is known to be found at rather high temperature: 400 °C (Berger and Velde, 1992; Smith and Barreiro, 1990; Wing et al., 2003) while the chlorite-epidote-paragenesis is formed in the range 350 to 200 °C (Norman et al., 1991). These conditions are compatible with that prevailing during the cooling stage following the intrusion of plutonic rocks.

5.2 Illitic alteration

Petrographic observations suggest that the propylitic alteration is overprinted by an illitic one in the upper part of the basement within 4-5 m below the unconformity. It is typically characterized by a massive replacement of all the primary and secondary minerals except the sericite zones in feldspars which seem to have been preserved. This could explain the co-existence of the $2M_1$ and 1M polytypes of the white micas fraction. The degree of replacement decreases with depth down to 7 m where illite is observed only in veins. Epidote and allanite have totally disappeared while chlorite seems to remains up to the unconformity. However, its composition changes becoming iron-richer composition. This indicates that it has recrystallized in a more stable version considering the local chemical condition imposed by the fluid responsible of the illitic alteration. As shown by the strong decrease of the ΔCaO and ΔNa_2O ratios on one hand and the increase of the ΔK_2O ones on the other hand, it appears that the illitic alteration induces more important chemical changes of the rocks that the propylitic one did (Fig. 8). It is obvious that it operates in an open system in which the fluids have flowed. The mineral

similarities between illite in the most altered basement samples and the upper sandstones militate for extensive chemical exchanges driven by the diagenetic fluids along the unconformity. The very low thorium content of the small euhedral monazite crystals indicates that they have crystallized at low temperature (Overstreet, 1960) and are probably synchronous with the illitic alteration.

5.3. Could a paleosol have been present along the unconformity?

Based on the study of fifty pre-Devonian rock units that have been described as paleosols, Rye and Holland (1998) proposed that five criteria must be respected to evidence the weathering effects: *(i)* the paleosol is developed on a homogeneous parent rock and has been preserved in place; *(ii)* textural; *(iii)* mineralogical; *(iiii)* chemical; *(iiiii)* soft sediments features. A geological formation that meets all these criteria is classified as definite paleosol; when all criteria are met but one it is likely a paleosol; all but two is a possible paleosol; not more than three criteria is unlikely a paleosol.

Considering the eight drill cores studied here, no petrographic features typical of a weathering process have been observed, even in the reddish samples from the GR31 or the GR20 drill cores. None of them contain any evidence of typical weathering processes such as primary phase recrystallization inside microsytems, clay translocation deposits (cutans) or increasing porosity toward the surface (Velde and Meunier, 2008). On the contrary, the rocks, irrespective of their petrographic properties, are all invaded by a single clay mineral phase: illite. If any physical traces of a weathering event have been preserved after the sediment deposition, they have been totally erased by the diagenetic alteration processes.

As it is the case for any water/rock interactions induced by pure water or diluted solution invasion, the most soluble components are leached out from the altered rock (Ca, Na, Mg) while the less soluble (Al, Ti) ones are concentrated and K is enriched (Fig. 8). These chemical characteristics do not meet the criteria proposed by Rye and Holland (1998). Consequently, the probability for a paleosol to have been formed on the unconformity surface before being buried under the sediments of the Franceville basin is very weak. The superimposition of an illitic alteration upon a previous propylitic one is the most probable scenario here. It is supported by the distinct chemical trends evidenced by plotting the bulk rock compositions in the Al_2O_3-CaO, Na_2O, K_2O-FeO, MgO system (Fig. 15). Two trends are clearly separated: (i) a shift toward the epidote-chlorite assemblage typical of the propylitic alteration or magmatic differentiation; (ii) a shift toward the illite pole. The two different chemical pathways are coherent with the progressive upward variation of Rb, Cs and Sr amounts which are increasing and decreasing respectively (Fig. 9). The same contrasted chemical behavior is also observed for the REE distribution: the amounts of the light ones (LREE) do not vary during the propylitic alteration while they are leached out during the illitic event (Fig. 9 and 10). This is also coherent with the disappearance of the allanite crystals which could be related to the percolation of oxidizing diagenetic fluids invading the basement from the overlying sedimentary basin through the unconformity (Cuney and Mathieu, 2000).

The negative $\delta^{13}C$ values of calcite crystals in veins indicate that the diagenetic fluids involved in the illitization process were mixed with organic compounds deriving from oil maturation in the FB sediments (Gauthier-Lafaye and Weber, 1989; Weber and Gauthier-Lafaye, 2013).

5.4. Timing of alteration events.

The isotopic U-Pb data gathers into three major dating groups. The oldest one, from 2998 ± 25 Ma to 2922 ± 24 Ma is consistent with the age of plutonic intrusions forming the basement. The 2621 ± 30 Ma intermediate group might correspond to the hydrothermal propylitic event related to the intrusion of the neoarchean plutonic bodies. It is to be noticed that the dating obtained here from monazite crystals is coherent with that measured in altered biotites using the K-Ar method: 2696 ± 60 Ma (Bonhomme et al., 1978). The youngest group, i.e. 1870 ± 26 Ma, has been measured on newly formed monazites from the illitized zone. Their extremely low Th contents reflect a crystallization process under low temperature conditions. It is consistent with the diagenetic event of the Franceville basin (Bonhomme et al., 1982).

6. Conclusion

The mineralogical and geochemical studies of the basement of the Franceville Basin along a nearly E-W profile show that the basement is composed of different plutonic rocks. Dating obtained from 8 drill holes give Archean ages (3.0 – 2.9 Ga) similar to the ones obtained on rocks outcropping in the Chaillu Massif. No metasedimentary formations have been intersected. Most of these rocks present evidences of a propylitic alteration which postdate any ductile deformation and which may be associated to the intrusion of some Neoarchean plutonic rocks at about 2.6 to 2.7 Ga (Thiéblemont et al., 2009). The mineral reactions produced a Mg chlorite + epidote + allanite + titanite paragenesis typical of nearly close systems: no significant mobility of the major elements suggesting weak Water/Rocks ratios. Then, a massive illitic alteration associated with hematization, has transformed the previously propylitized rocks over a thickness of 2 to 5 m below the unconformity in the Franceville basin. It has been triggered by the percolation of oxidizing diagenetic fluids from the FA conglomeratic-sandstone formation at the base of the sedimentary basin through the unconformity. Similar fluid invasions have been described in other

basins: Southern Norway (Munz et al., 1995; Oliver et al., 2006), Spain (Bouch et al., 2006), France, Northwestern Massif Central (Munoz et al., 1999), Athabasca, Canada (Richard et al., 2013) and Kombolgie, Australia (Derome et al., 2003). Most of the major and light Rare Earth elements have been heavily depleted. This is particularly the case for Ca, Na and Mg while Al amounts are roughly preserved. No paleosol chemical or petrographical traces have been detected here. The calcite $\delta^{13}C$ values confirm the diagenetic origin for the fluids which have percolated into the basement. They were also responsible of the uranium transfer and deposition in the vicinity of the organic-rich sediments of the FB formation which gave the natural nuclear reactors (Gauthier-Lafaye and Weber, 2003; Mathieu et al., 2000).

AKNOWLEDGMENT

We thank the Gabonese Government, the Sylvia Bongo Foundation, Région Poitou-Charentes, FEDER program, CNRS-INSU and University of Poitiers for their financial supports. Wealsothank the « Direction Générale des Mines et de la Géologie du Gabon » (DGMG) for itstechnical support.

REFERENCES

Achterbergh, E., Ryan, C.G., Jackson, S.E., and Griffin, W.L., 2001, Data reduction software for LA-ICP-MS: In: Laser ablation-ICPMS in the earth science. P. Sylvester ed. Mineralogical Association of Canada, v. 29, .

Albani, A.E., Bengtson, S., Canfield, D.E., Bekker, A., Macchiarelli, R., Mazurier, A., Hammarlund, E.U., Boulvais, P., Dupuy, J.-J., Fontaine, C., Fürsich, F.T., Gauthier-Lafaye, F., Janvier, P., Javaux, E., Ossa, F.O., Pierson-Wickmann, A.-C., Riboulleau, A., Sardini, P., Vachard, D., Whitehouse, M., and Meunier, A., 2010, Large colonial

organisms with coordinated growth in oxygenated environments 2.1[thinsp]Gyr ago: Nature, v. 466, p. 100-104.

Berger, G., and Velde, B., 1992, Chemical parameters controlling the propylitic and argillic alteration process: Stuttgart, ALLEMAGNE, Schweizerbart.

Bonhomme, M., Leclerc, J., and Weber, F., 1978, Etudes radiochronologique complémentaire de la série du Francevillien et de son environnement: In: IAEA, editors. Les réacteurs de fission naturels, Vienne,, p. 19-23.

Bonhomme, M.G., Gauthier-Lafaye, F., and Weber, F., 1982, An example of lower proterozoic sediments: The Francevillian in Gabon: Precambrian Research, v. 18, p. 87-102.

Bouch, J., Naden, J., Shepherd, T., McKervey, J., Young, B., Benham, A., and Sloane, H., 2006, Direct evidence of fluid mixing in the formation of stratabound Pb–Zn–Ba–F mineralisation in the Alston Block, North Pennine Orefield (England): Mineralium Deposita, v. 41, p. 821-835.

Bouton, P., Thiéblemont, D., Gouin, J., Cocherie, A., Guerrot, C., Tegyey, M., Préat, A., Simo Ndounze, S., and Moussavou, M., 2009, Notice explicative de la carte géologique de la République du Gabon à 1/200 000, feuille Franceville-Boumango: . Edition DGMG-Ministère des Mines, du Pétrole, des Hydrocarbures, Libreville,, p. 79 p.

Caen-Vachette, M., Vialette, Y., Bassot, J.P., and Vidal, P., 1988, Apport de la géochronologie isotopique à la connaissance de la géologie gabonaise: Chronique de Recherche Minière, v. 491, p. 35-54.

.

Card, K.D., 1978, Metamorphism of the Middle Precambrian (Aphebian) rocks of the eastern southern Province: Metamorphism in the Canadian Shield; by Fraser, J A (ed.); Heywood, W W (ed.); Geological Survey of Canada,, v. 78-10, p. 269-282.

Chevallier, L., Makanga, J.F., and Thomas, R.J., 2002, Notice explicative de la Carte géologique de la République Gabonaise à 1/ 1 000 000: Editions DGMG Gabon, p. 195.

Cuney, M., and Mathieu, R., 2000, Extreme light rare earth element mobilization by diagenetic fluids in the geological environment of the Oklo natural reactor zones, Franceville basin, Gabon: Geology, v. 28, p. 743-746.

Debon, F., and Le Fort, P., 1983, A chemical–mineralogical classification of common plutonic rocks and associations: Earth and Environmental Science Transactions of the Royal Society of Edinburgh, v. 73, p. 135-149.

Derome, D., Cuney, M., Cathelineau, M., Fabre, C., Dubessy, J., Bruneton, P., and Hubert, A., 2003, A detailed fluid inclusion study in silicified breccias from the Kombolgie sandstones (Northern Territory, Australia): inferences for the genesis of middle-

Proterozoic unconformity-type uranium deposits: JOURNAL OF GEOCHEMICAL EXPLORATION, v. 80, p. 259-275.

Gasquet, D., Bertrand, J.-M., Paquette, J.-L., Lehmann, J., Ratzov, G., De Ascenção Guedes, R., Tiepolo, M., Boullier, A.-M., Scaillet, S., and Nomade, S., 2010, Miocene to Messinian deformation and hydrothermal activity in a pre-Alpine basement massif of the French western Alps: new U-Th-Pb and argon ages from the Lauzière massif: Bulletin de la Societe Geologique de France, v. 181, p. 227-241.

Gauthier-Lafaye, F., 1986, Les gisements d'uranium du Gabon et les reacteurs d'Oklo. Modèle métallogénique de gîtes à fortes teneurs du protérozoique inférieur: Thèse de Doctorat d'Etat, Université de Strasbourg, p. 206.

Gauthier-Lafaye, F., Holliger, P., and Blanc, P.L., 1996, Natural fission reactors in the Franceville basin, Gabon: A review of the conditions and results of a "critical event" in a geologic system: Geochimica et Cosmochimica Acta, v. 60, p. 4831-4852.

Gauthier-Lafaye, F., and Weber, F., 1989, The Francevillian (Lower Proterozoic) uranium ore deposits of Gabon: Economic Geology, v. 84, p. 2267-2285.

Gauthier-Lafaye, F., and Weber, F., 2003, Natural nuclear fission reactors: time constraints for occurrence, and their relation to uranium and manganese deposits and to the evolution of the atmosphere: Precambrian Research, v. 120, p. 81-100.

Haubensack, C., 1981, Environnement des grès protérozoïques et des indices uranifères du secteur Kiéné dans le bassin de Franceville (République Gabonaise): aspects sédimentologiques et géochimiques.

Huang, H., Polat, A., and Fryer, B.J., 2013, Origin of Archean tonalite–trondhjemite–granodiorite (TTG) suites and granites in the Fiskenæsset region, southern West Greenland: Implications for continental growth: Gondwana Research, v. 23, p. 452-470.

Jackson, S.E., Pearson, N.J., Griffin, W.L., and Belousova, E.A., 2004, The application of laser ablation-inductively coupled plasma-mass spectrometry to in situ U–Pb zircon geochronology: Chemical Geology, v. 211, p. 47-69.

Lowell, J.D., and Guilbert, J.M., 1970, Lateral and vertical alteration-mineralization zoning in porphyry ore deposits: Economic Geology, v. 65, p. 373-408.

Martin, H., 1986, Effect of steeper Archean geothermal gradient on geochemistry of subduction-zone magmas: Geology, v. 14, p. 753-756.

Martin, H., 1987, Petrogenesis of Archaean trondhjemites, tonalites, and granodiorites from eastern Finland: major and trace element geochemistry: Journal of Petrology, v. 28, p. 921-953.

Martin, H., Moyen, J.-F., and Rapp, R., 2010, The sanukitoid series: magmatism at the Archaean–Proterozoic transition, Sixth Hutton Symposium on the Origin of Granites and

Related Rocks: Proceedings of a Symposium Held in Stellenbosch, South Africa, 2-6 July 2007, Volume 472, Cambridge Univ Press, p. 15.

Mathieu, R., 1999, Reconstitution des paléocirculations fluides et des migrations élémentaires dans l'environnement des réacteurs nucléaires naturels d'Oklo (Gabon) et des Argilites de Tournemire (France). : Thèse de Doctorat, Institut National Polytechnique, Lorraine, p. 518.

Mathieu, R., Cuney, M., and Cathelineau, M., 2000, Geochemistry of palaeofluids circulation in the Franceville basin and around Oklo natural nuclear reaction zones (Gabon): JOURNAL OF GEOCHEMICAL EXPLORATION, v. 69, p. 245-249.

Mercadier, J., Richard, A., Boiron, M.-C., Cathelineau, M., and Cuney, M., 2010, Migration of brines in the basement rocks of the Athabasca Basin through microfracture networks (P-Patch U deposit, Canada): Lithos, v. 115, p. 121-136.

Muller, W., Shelley, M., Miller, P., and Broude, S., 2009, Initial performance metrics of a new custom-designed ArF excimer LA-ICPMS system coupled to a two-volume laser-ablation cell: Journal of Analytical Atomic Spectrometry, v. 24, p. 209-214.

Munoz, M., Boyce, A.J., Courjault-Rade, P., Fallick, A.E., and Tollon, F., 1999, Continental basinal origin of ore fluids from southwestern Massif central fluorite veins (Albigeois, France): evidence from fluid inclusion and stable isotope analyses: Applied Geochemistry, v. 14, p. 447-458.

Munz, I.A., Yardley, B.W.D., Banks, D.A., and Wayne, D., 1995, Deep penetration of sedimentary fluids in basement rocks from southern Norway: Evidence from hydrocarbon and brine inclusions in quartz veins: Geochimica et Cosmochimica Acta, v. 59, p. 239-254.

Murakami, T., Kasama, T., and Utsunomiya, S., 2011, Early Proterozoic weathering processes under low O2 conditions reconstructed from a 2.45 Ga paleosol in Pronto, Canada: American Mineralogist, v. 96, p. 1613-1623.

Naudet, R., 1991, Des Réacteurs Nucléaires Fossiles: Paris (coll. CEA).

Nedachi, Y., Nedachi, M., Bennett, G., and Ohmoto, H., 2005, Geochemistry and mineralogy of the 2.45 Ga Pronto paleosols, Ontario, Canada: Chemical Geology, v. 214, p. 21-44.

Nesbitt, H.W., 1979, Mobility and fractionation of rare earth elements during weathering of a granodiorite: Nature, v. 279, p. 206-210.

Norman, D.K., Parry, W.T., and Bowman, J.R., 1991, Petrology and geochemistry of propylitic alteration at Southwest Tintic, Utah: Economic Geology, v. 86, p. 13-28.

Ohmoto, H., 1996, Evidence in pre–2.2 Ga paleosols for the early evolution of atmospheric oxygen and terrestrial biota: Geology, v. 24, p. 1135-1138.

Ohmoto, H., and Kerrick, D.M., 1977, Devolatilization equilibria in graphitic systems: American Journal of Science, v. 277, p. 1013-1044.

Oliver, N.H.S., McLellan, J.G., Hobbs, B.E., Cleverley, J.S., Ord, A., and Feltrin, L., 2006, 100th Anniversary Special Paper: Numerical Models of Extensional Deformation, Heat Transfer, and Fluid Flow across Basement-Cover Interfaces during Basin-Related Mineralization: Economic Geology, v. 101, p. 1-31.

Overstreet, W., 1960, Metamorphic grade and the abundance of ThO2 in monazite: US Geological Survey Professional Paper, p. 55-57.

Paquette, J.L., and Tiepolo, M., 2007, High resolution (5 μm) U–Th–Pb isotope dating of monazite with excimer laser ablation (ELA)-ICPMS: Chemical Geology, v. 240, p. 222-237.

Prian, J.P., and Johan, V., 1989, Contribution à la reconnaissance géologique et pétrographique de l'Archéen du massif du Chaillu et du Francevillien du Bassin des Abeilles (région deKoulamoutou – Lastoursville, Gabon): Rapport BRGM 89 GAB 079 GEO, v. 55 p.

Richard, A., Boulvais, P., Mercadier, J., Boiron, M.-C., Cathelineau, M., Cuney, M., and France-Lanord, C., 2013, From evaporated seawater to uranium-mineralizing brines: Isotopic and trace element study of quartz–dolomite veins in the Athabasca system: Geochimica et Cosmochimica Acta, v. 113, p. 38-59.

Rye, R., and Holland, H.D., 1998, Paleosols and the evolution of atmospheric oxygen; a critical review: American Journal of Science, v. 298, p. 621-672.

Sère, V., 1996, Géochimie des minéraux néoformés à Oklo (Gabon): histoire géologique du bassin d'Oklo, une contribution pour les études de stockages géologiques de déchets radioactifs: Thèse de Doctorat, Université de Paris VII, p. 278.

Seydoux-Guillaume, A.-M., Paquette, J.-L., Wiedenbeck, M., Montel, J.-M., and Heinrich, W., 2002, Experimental resetting of the U–Th–Pb systems in monazite: Chemical Geology, v. 191, p. 165-181.

Smith, H., and Barreiro, B., 1990, Monazite U-Pb dating of staurolite grade metamorphism in pelitic schists: Contributions to Mineralogy and Petrology, v. 105, p. 602-615.

Stern, R., 1989, Petrogenesis of the Archean sanukitoid suite: State university at Stony Brook, New York, p. 275 p.

Thiéblemont, D., Castaing, C., Billa, M., Bouton, P., and and Préat, A., 2009, Notice explicative de la Carte géologique et des Ressources minérales de la République Gabonaise à 1/1000 000: Editions DGMG - Ministère des Mines, du Pétrole, des Hydrocarbures, Libreville, p. 384.

Thomas, R.J., Makanga, J.F., and Chevallier, L., 2001, Carte géologique de la République Gabonaise à 1/ 1 000 000: 2eme Editions, DGMG Gabon.

593 Titley, S.R., Thompson, R.C., Haynes, F.M., Manske, S.L., Robison, L.C., and White, J.L., 1986,
594 Evolution of fractures and alteration in the Sierrita-Esperanza hydrothermal system, Pima
595 County, Arizona: Economic Geology, v. 81, p. 343-370.

596 Velde, B., and Meunier, A., 2008, The Origin of Clay Minerals in Soils and Weathered Rocks:
597 With 23 Tables, Springer.

598 Weber, F., 1968, Une série précambrienne du Gabon, le Francevillien: sédimentologie,
599 géochimie, relations avec lkes gîtes minéraux associés, Université de Strasbourg.

600 Weber, F., and Gauthier-Lafaye, F., 2013, No proof from carbon isotopes in the Francevillian
601 (Gabon) and Onega (Fennoscandian shield) basins of a global oxidation event at 1980–
602 2090 Ma following the Great Oxidation Event (GOE): Comptes Rendus Geoscience, v.
603 345, p. 28-35.

604 White, A.F., Bullen, T.D., Schulz, M.S., Blum, A.E., Huntington, T.G., and Peters, N.E., 2001,
605 Differential rates of feldspar weathering in granitic regoliths: Geochimica et
606 Cosmochimica Acta, v. 65, p. 847-869.

607 Wing, B., Ferry, J., and Harrison, T.M., 2003, Prograde destruction and formation of monazite
608 and allanite during contact and regional metamorphism of pelites: petrology and
609 geochronology: Contributions to Mineralogy and Petrology, v. 145, p. 228-250.

610

611 **Figure captions**

612

613 **Fig. 1**: Simplified geological map of Franceville basin and location of the studied region
614 (modified after Bros et al, 1993).

615

616 **Fig. 2**: (a) Location of the studied drill cores (KA13, GR1, GR5, GR20, GR23, GR31, GR 43 and
617 KA6) close to Kaya-Kaya fault in the Franceville basin; (b) Simplified geological logs of the
618 studied drill cores.

619

620 **Fig. 3**: Bulk rock chemical compositions in the Debon and Le Fort diagram (1983). In brackets
621 (L.O.I.), Q = normative quartz, P = normative feldspars. (**a**) GR20 and GR31 drill cores, (**b**)
622 GR23, KA6 drill cores. Dot arrow = magmatic differentiation trend. The white triangles represent
623 the average compositions of the diorite quartzite (dq), tonalite (to), granodiorites (gd), and
624 adamellite (ad)

625

626 **Fig. 4**: Chondrite-normalized rare earth element patterns of the least altered rocks.
627 Adamellite(KA6 472), Granodiorite (KA6 445, GR31 873 and GR31 866), Tonalite (KA6 467,
628 KA6 454, KA6 449, KA6 444, KA6 438, GR23 640), Diorite (KA6 462).
629
630 **Fig. 5**: Photomicrographs of the granitoids affected by propylitic alteration: (**a**) biotite is
631 completely replaced by the chlorite associated to rod shaped allanite and titanite, backscattered
632 electron SEM image; (b) sericitization of the feldspar, chloritization of biotite and chlorite calcite
633 sequence of fissure infilling. chloritized biotite = chl biot, chlorite = chl, allanite = All, titanite =
634 tin, feldspar = Felds, calcite = Cal, QZ = quartz.
635
636 **Fig. 6:** Photomicrographs of illitization features in granitoids; (a) feldspars are completely
637 replaced by illite while quartz (Qz) are cracked and enveloped by illitic matrix; (**b**) The
638 chloritized biotite is partially to totally replaced by the Fe-oxide + phengite (Phg) assemblage; (**c**)
639 fracture filled by calcite (cal); (**d**) Cementation in the FA sandstone by anhydrite.
640
641 **Fig. 7**: Evolution of Δ LOI with depth of tonalite.
642
643 **Fig. 8**: Plot of ΔSiO_2, ΔAl_2O_3, ΔCaO, ΔNa_2O, ΔFe_2O_3, ΔMgO, ΔK_2O versus ΔLOI of
644 propylitized (black diamond) and illitized (open circle) tonalite.
645 **Fig. 9**: Plot of ΔRb, ΔSr, ΔLa, ΔCe, ΔCs, ΔTh, ΔU versus ΔLOI of propylitized (black diamond)
646 and illitized (open circle) tonalites.
647
648 **Fig. 10**: Evolution of the chondrite-normalized rare earth element patterns of the granitoids, from
649 the least altered to the most altered (illitized) granitoids. Open square = illitized granitoids, black
650 losange = superimposed illitic on propylitic alteration, open circle = least altered and propylitized
651 granitoids.
652
653 **Fig. 11**: (**a**) Evolution of the XRD patterns of the < 2 µm fractions from KA6 467 m (granitoids)
654 to KA6 436 m (sandstone); (**b**) Evolution of the XRD patterns of chlorite from KA6 467 m
655 tonalite), to KA6 438 drill core < 2µm fraction in oriented glycol saturation preparations. Chl =
656 chlorite, ill = illite.

Fig. 12: (**a**) Representation of the four clay mineral domains in the MR^{3+}, $2R^{3+}$, $3R^{2+}$ triangle (Velde, 1985): illite, phengite (Ph), chlorite upper zone (chlup) and chlorite lower zone (chl_{low}), phengite + chlorite mixture (Ph + chl_{up}) domain. (**b**) Evolution of chemical compositions of the chlorites analyzed from the depth (lower zone) to the unconformity (upper zone) in the Fe/(Fe + Mg) versus Si diagram. Open diamond = chlorite of lower zone, open circles = chlorite of upper zone.

Fig. 13: Representation of Pb and U isotopic data in the $^{206}Pb/^{238}U$ versus $^{207}Pb/^{235}U$ diagram. MSWD = Mean Square Weighted Deviation. Monazites of KA6 437.85 sample.

Fig. 14: Representation of Pb and U isotopic data $^{207}Pb/^{206}Pb$ versus $^{206}Pb/^{238}U$ diagram. MSWD = Mean Square Weighted Deviation. Monazites of GR1 631 sample.

Fig. 15: (a) Representation of the alteration effects in the Al_2O_3 - CaO* + Na_2O + K_2O - FeO + MgO diagrams (Rainbird et al., 1990). CaO* = CaO of silicates. L.alt = least altered rocks, Pro + dif = propylitized rocks + magmatic differentiation, Ill. = analyzed illites, phg = analyzed phengites. Illite = theorical illite, Ka = kaolinite, Gi = Gibbsite. Black arrows indicate the least altered rock to-propylitized rock and the propylitized rock-to- illitized rock. (1) 2.6 Ga propylitic event, (2) 1.87 Ga late diagenetic (illitic) event**.**

Table captions

Table 1. Whole-rock geochemical data for the Archean granitoids at Kiéné area.

Table 2: Representative microprobe analyses of chlorites from the propylitic zone. The structural formulae are calculated on the 14 oxygen basis.

Table 3: Representative microprobe analyses of chlorites from the illitic zone. The structural 796 formulae are calculated on the 14 oxygen basis.

688 **Table 4**: Representative microprobe analyses of phengites from 797 the illitic zone. The
689 structural formulae are calculated on the 11 oxygen basis.
690
691 **Table 5**: Representative microprobe analyses of illites from the illitic zone. The structural
692 800 formulae are calculated on the 11 oxygen basis.
693
694 **Table 6**: Representative microprobe analyses of epidotes and allanites from the propylitic zone.
695 The structural formulae are calculated on the 12.5 oxygen basis.
696
697 **Table 7**: Representative microprobe analyses of monazites.
698
699 **Table 8**: Representative Laser-ICPMS analyses and age calculations of monazites (sample
700 805 KA6 437.85).
701
702 **Table 9**: Representative Laser-ICPMS analyses and age calculations of monazites (sample
703 807 GR1 631).
704
705 **Table 10**: $\delta^{13}C$ values (‰ PDB) and $\delta^{18}O$ (‰ SMOW) measured on six samples affected by
706 carbonated alteration.
707
708

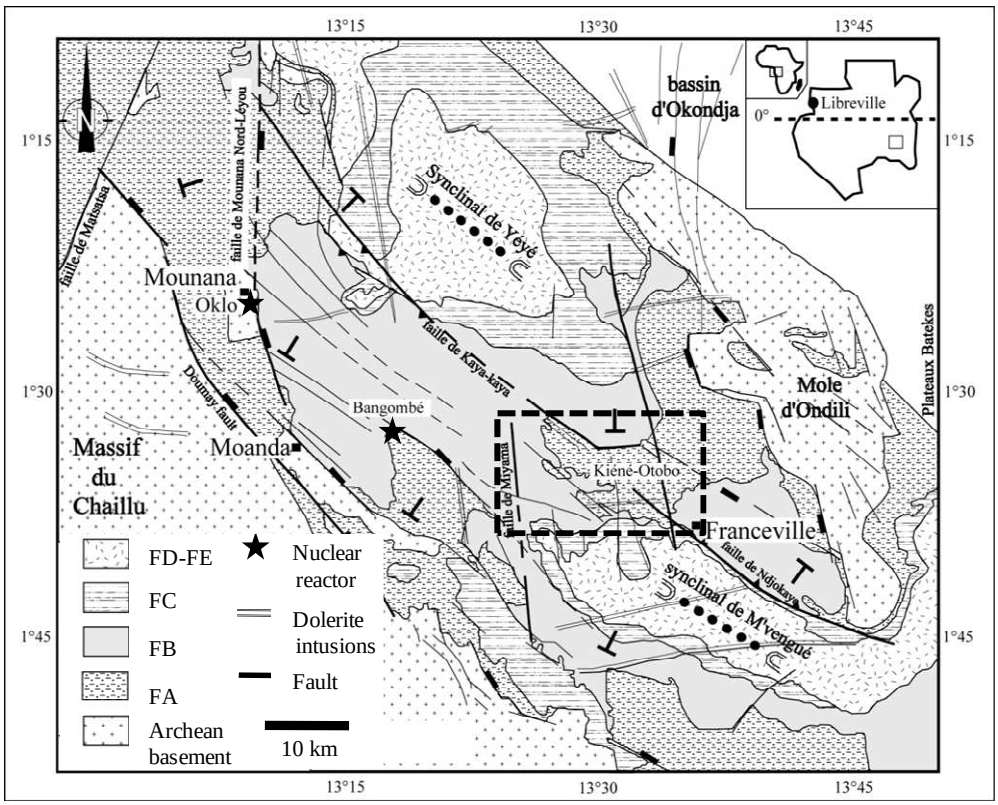

Figure 1

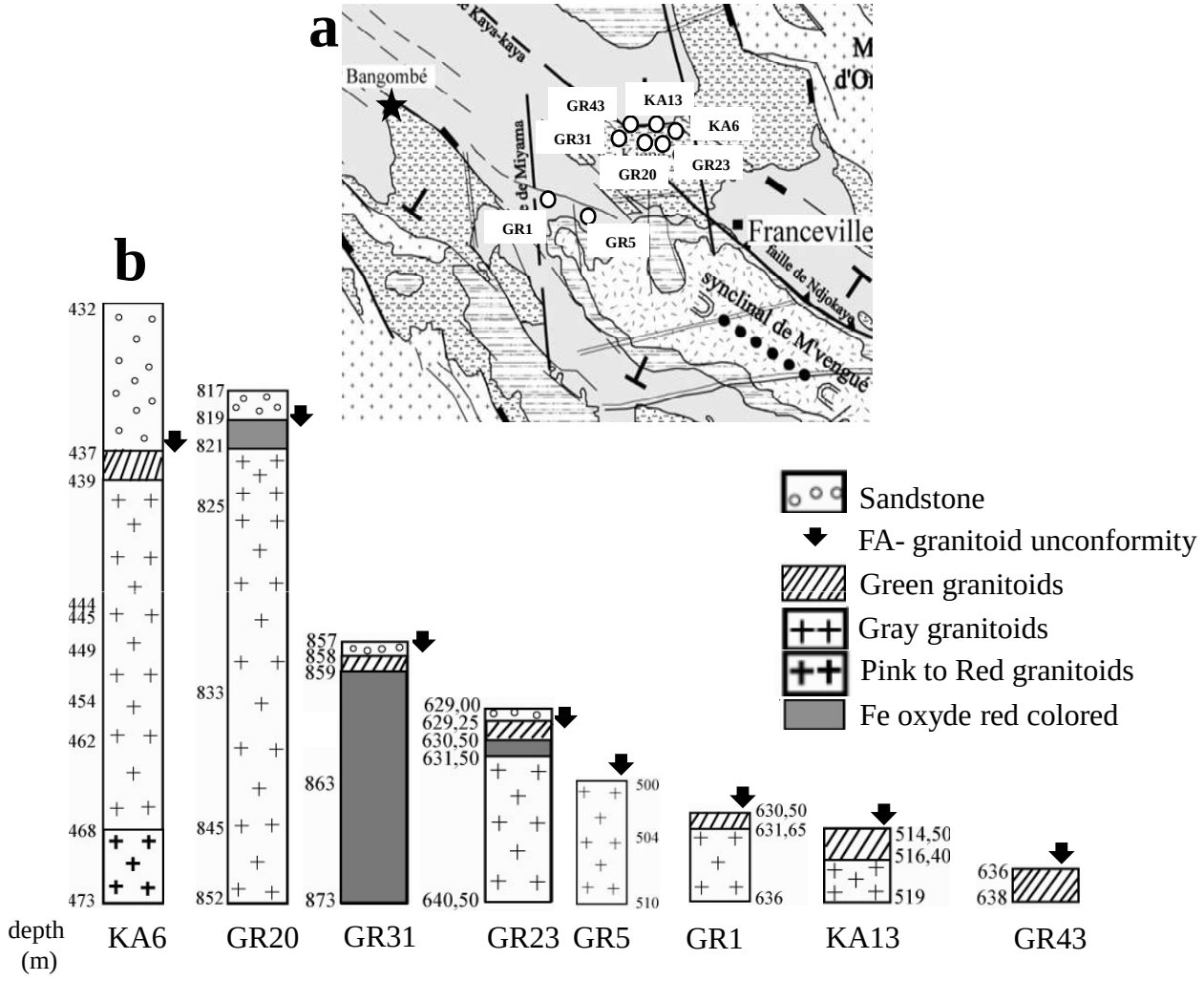
a
Bangombé
Kaya-kaya
GR43
KA13
KA6
GR31
GR20
GR23
GR1
GR5
Franceville
faille de Ndjokaya
synclinal de M'vengué
b
Sandstone
FA- granitoid unconformity
Green granitoids
Gray granitoids
Pink to Red granitoids
Fe oxyde red colored
depth (m)
KA6
GR20
GR31
GR23
GR5
GR1
KA13
GR43
432
437
439
444
445
449
454
462
468
473
817
819
821
825
833
845
852
857
858
859
863
873
629,00
629,25
630,50
631,50
640,50
500
504
510
630,50
631,65
636
514,50
516,40
519
636
638

Figure 2

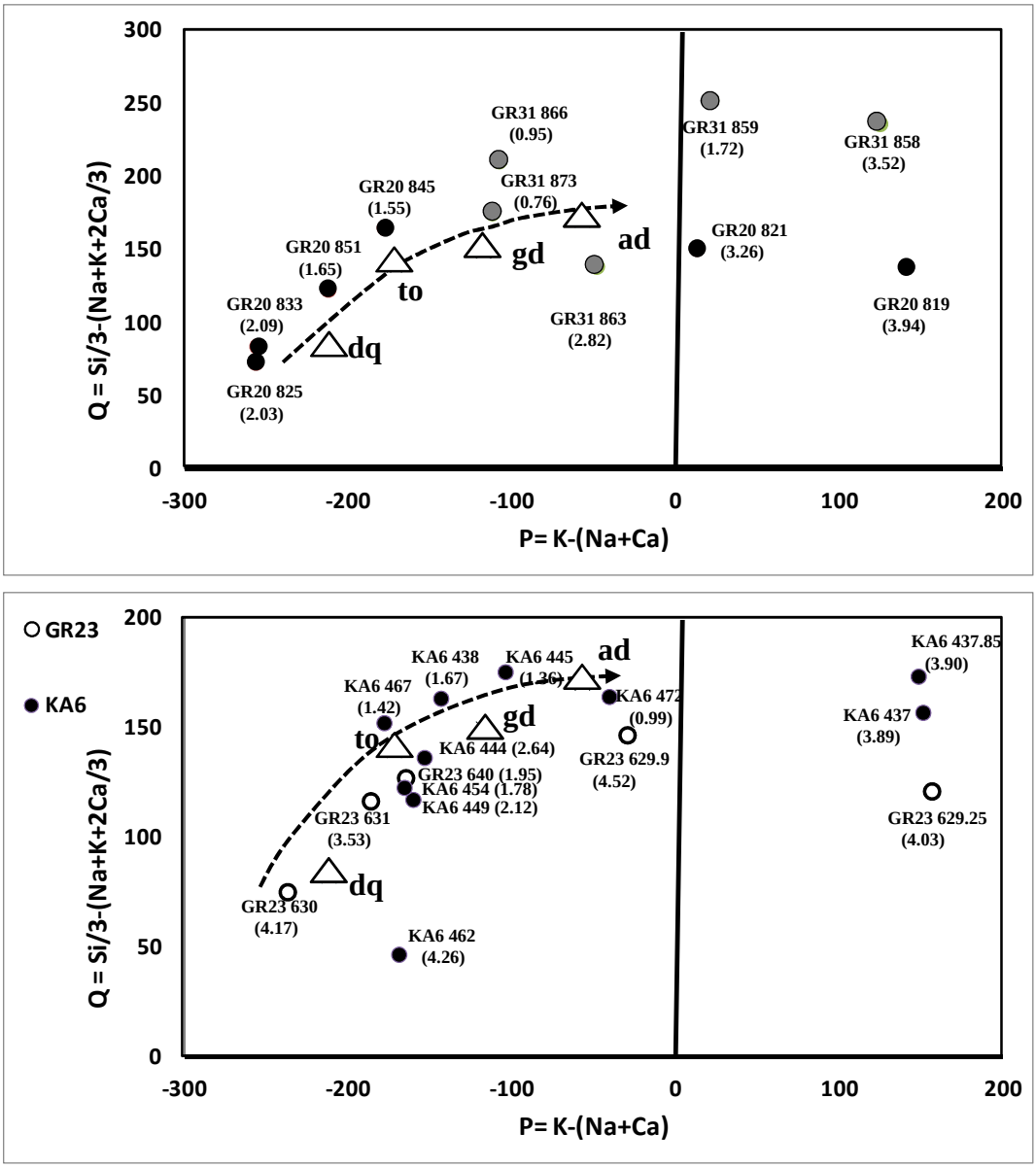

Figure 3

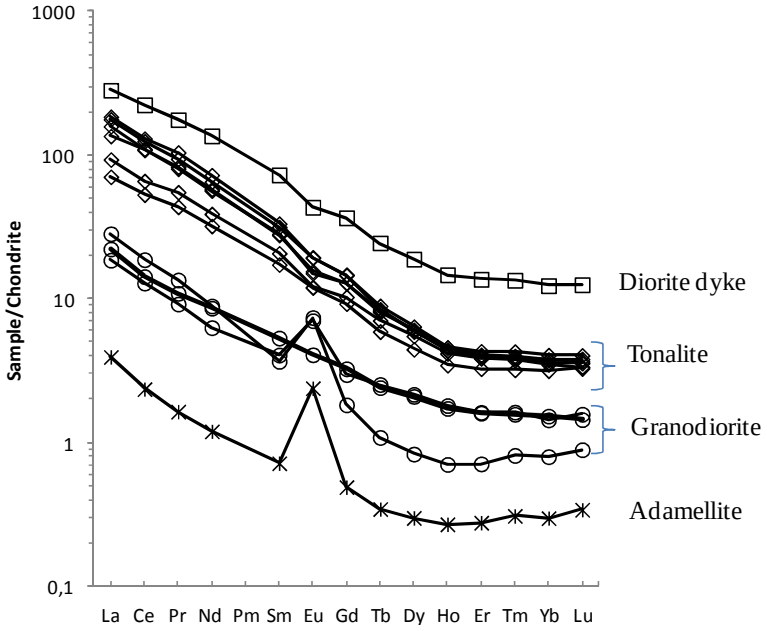

Figure 4

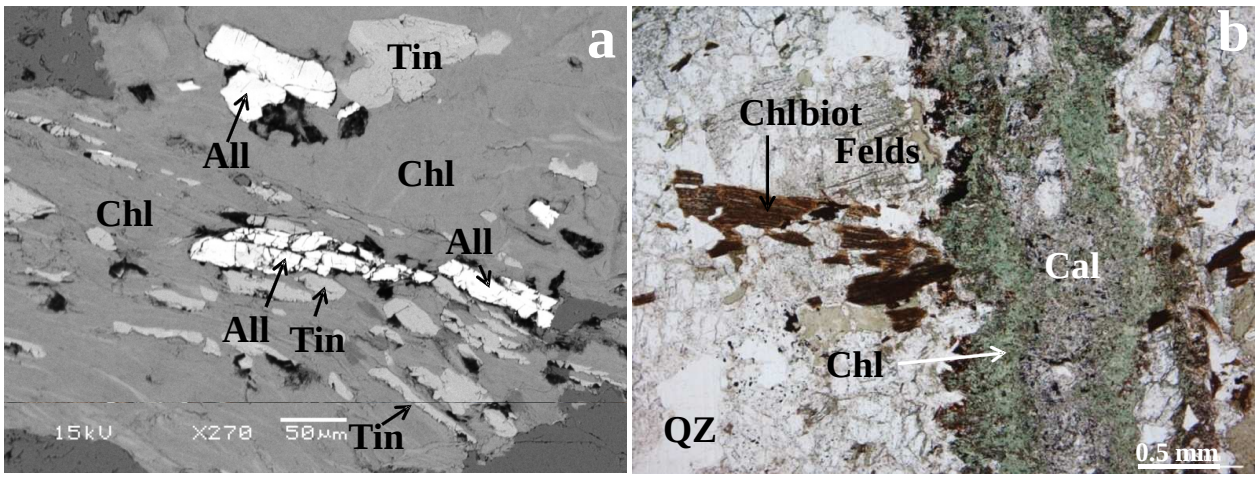

Figure 5

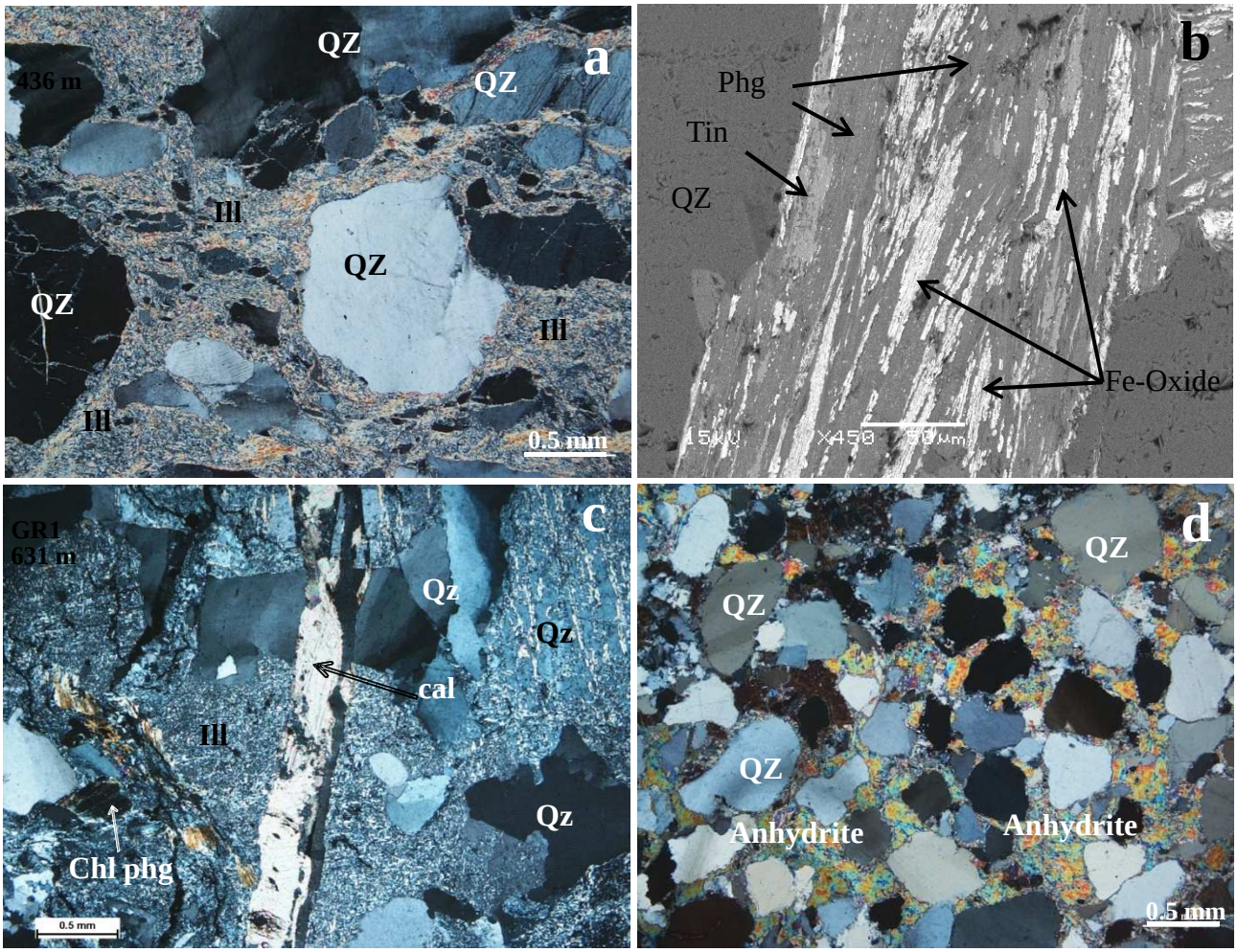

Figure 6

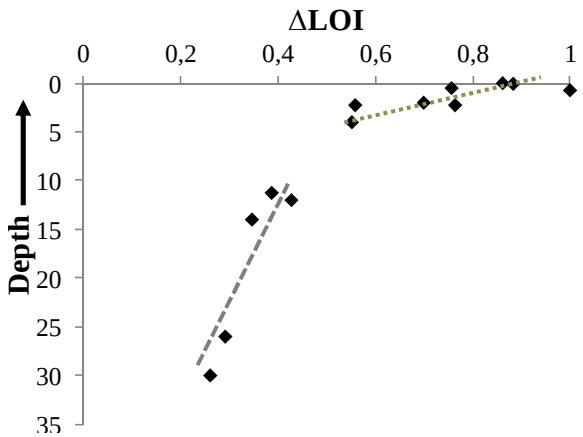

Figure 7

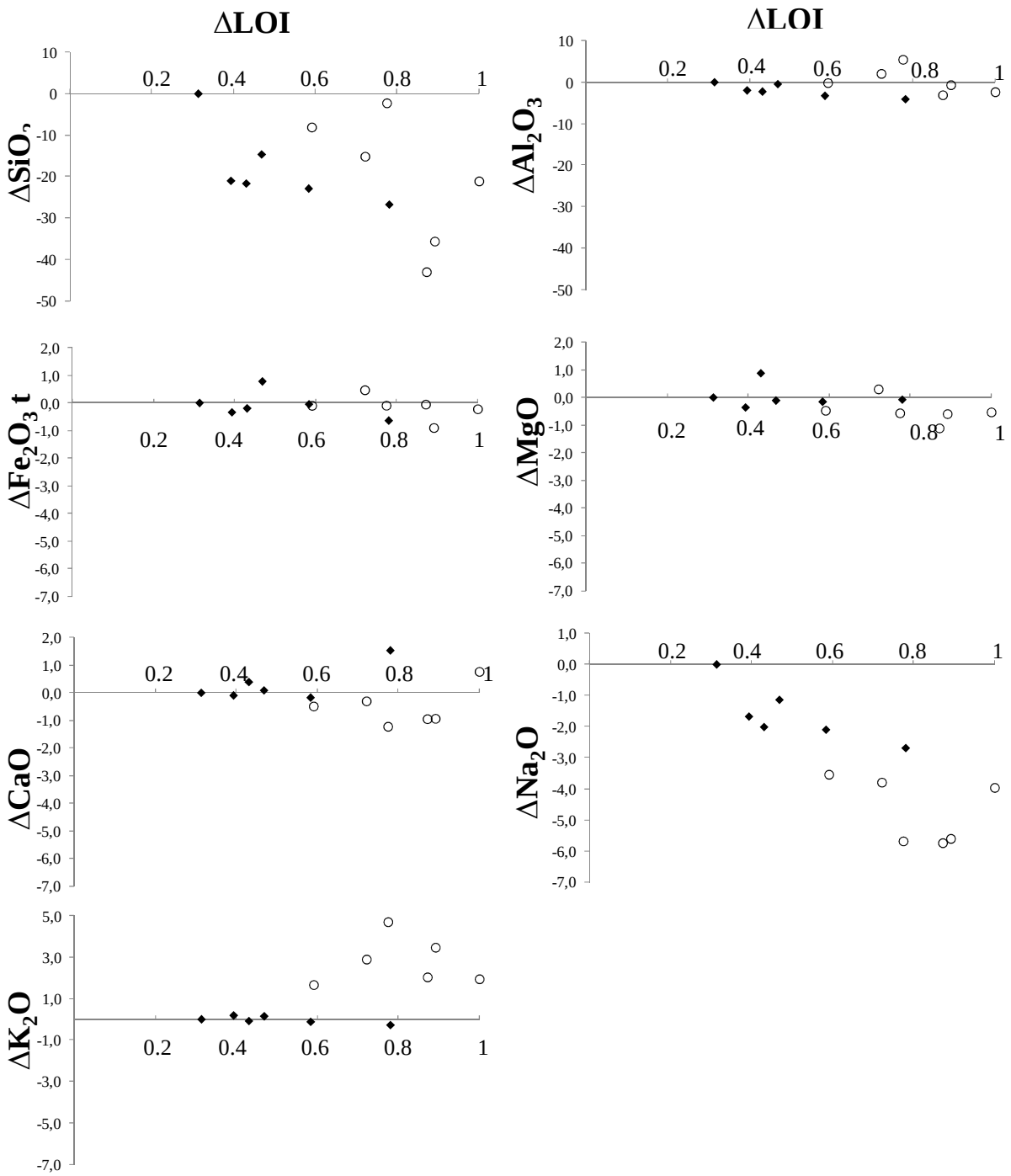

Figure 8

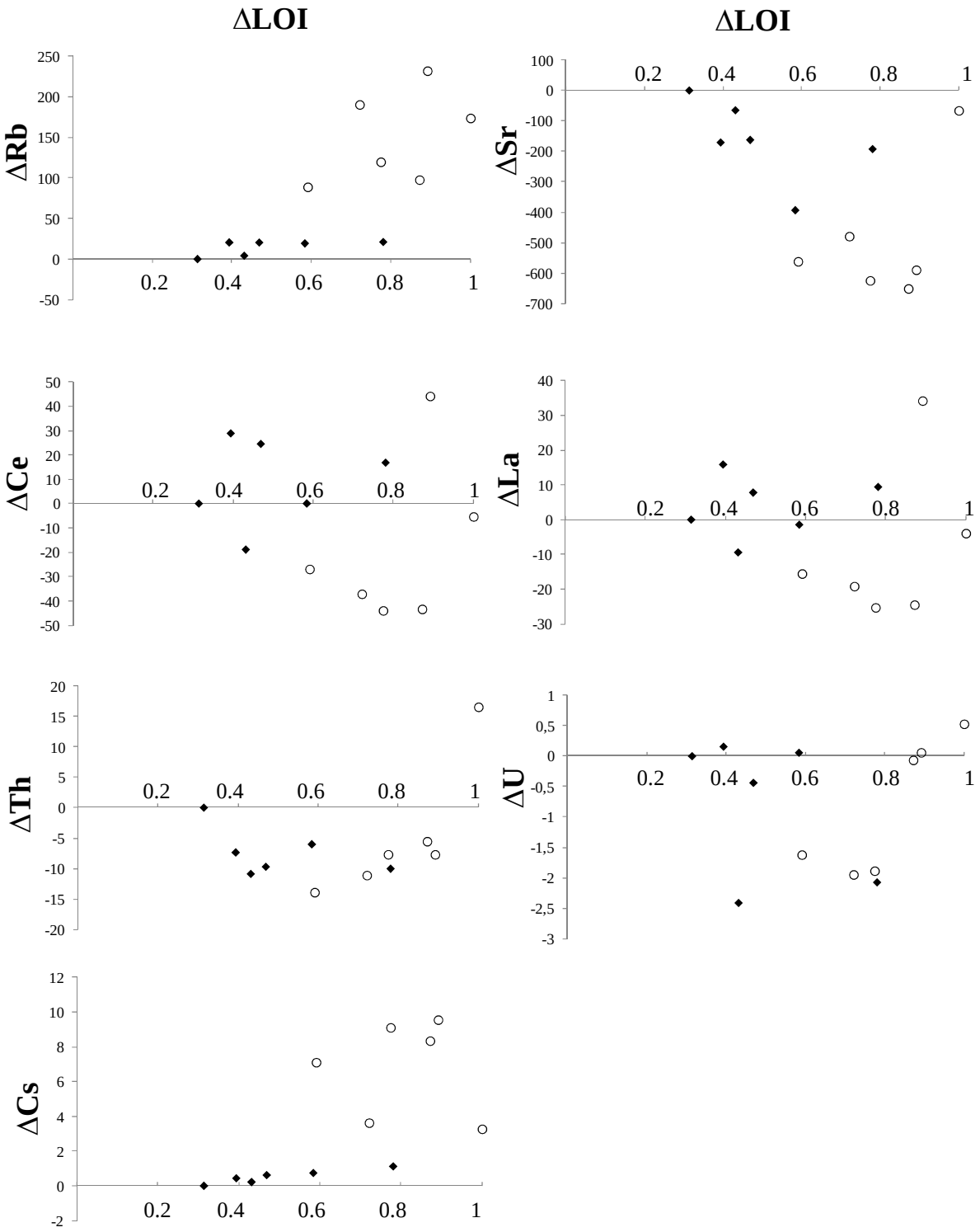

Figure 9

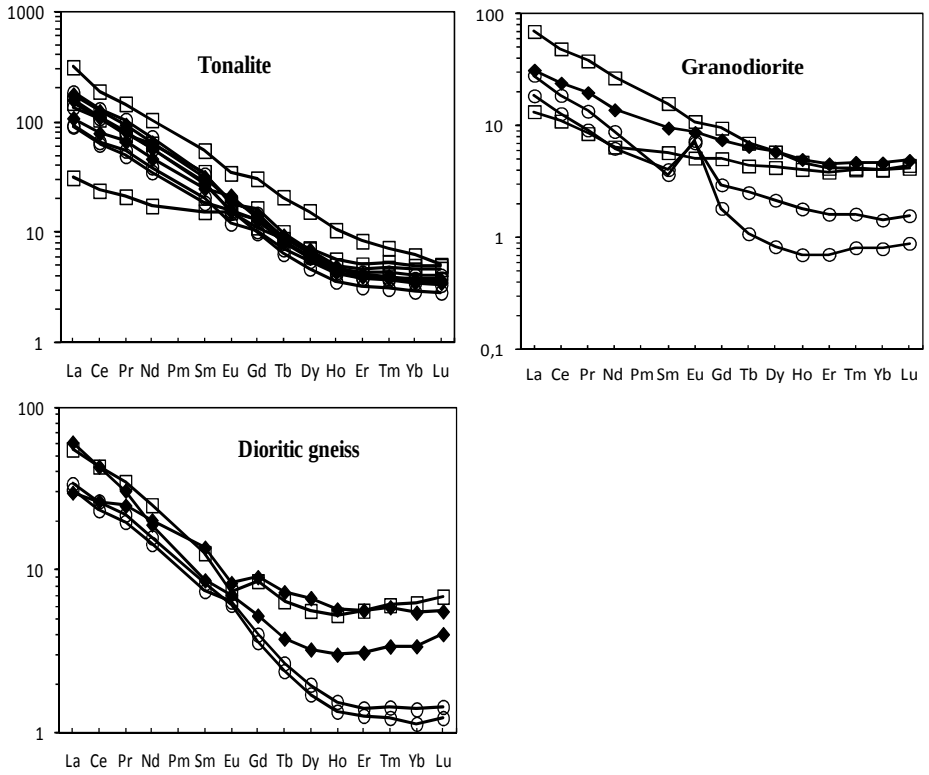

Figure 10

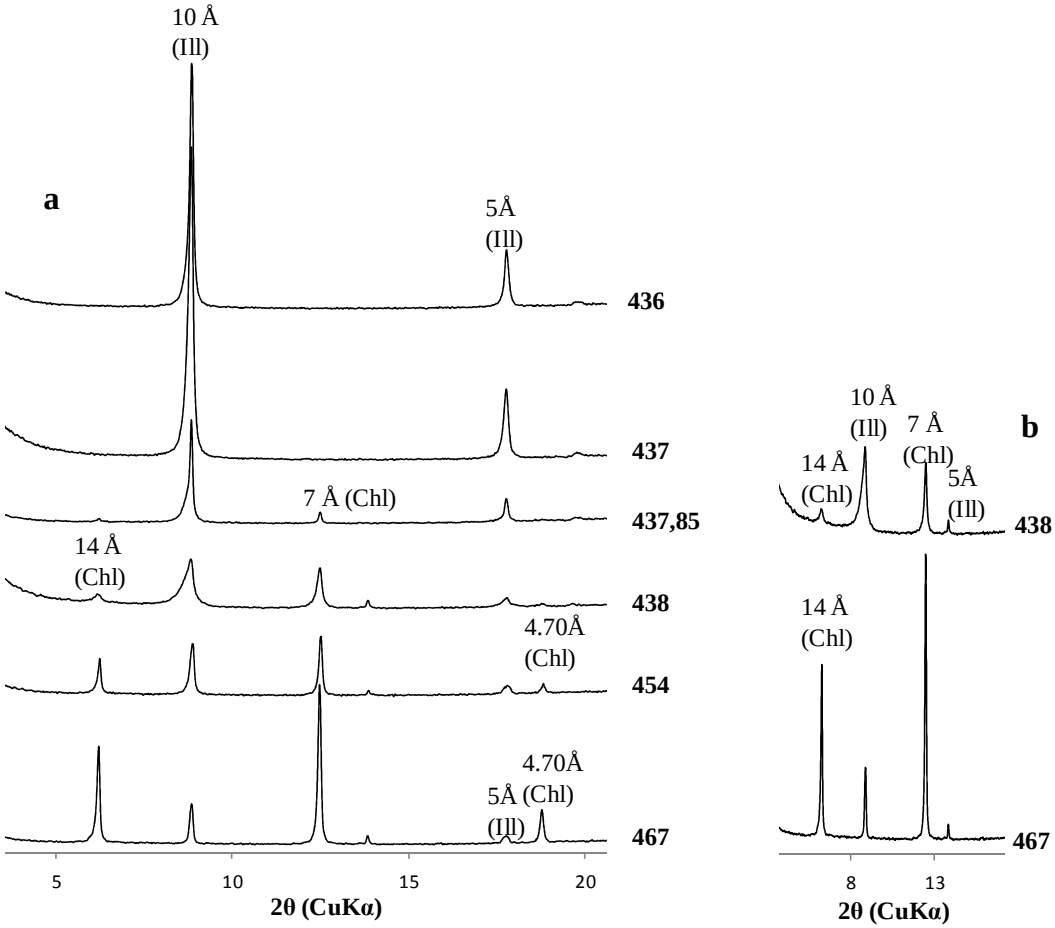

Figure 11

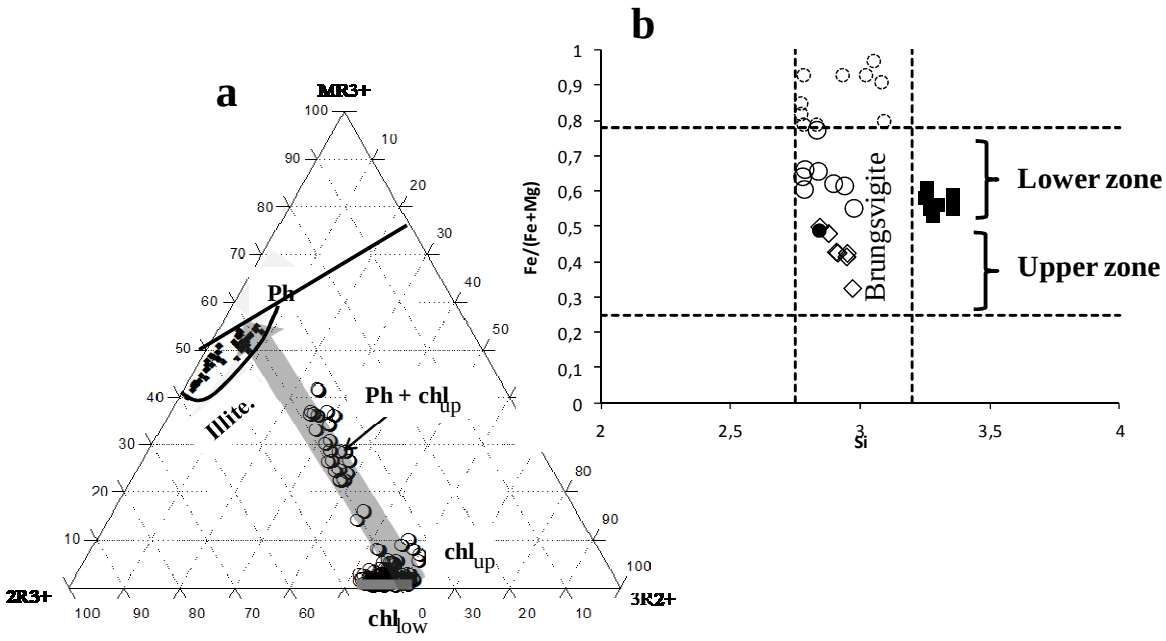

Figure 12

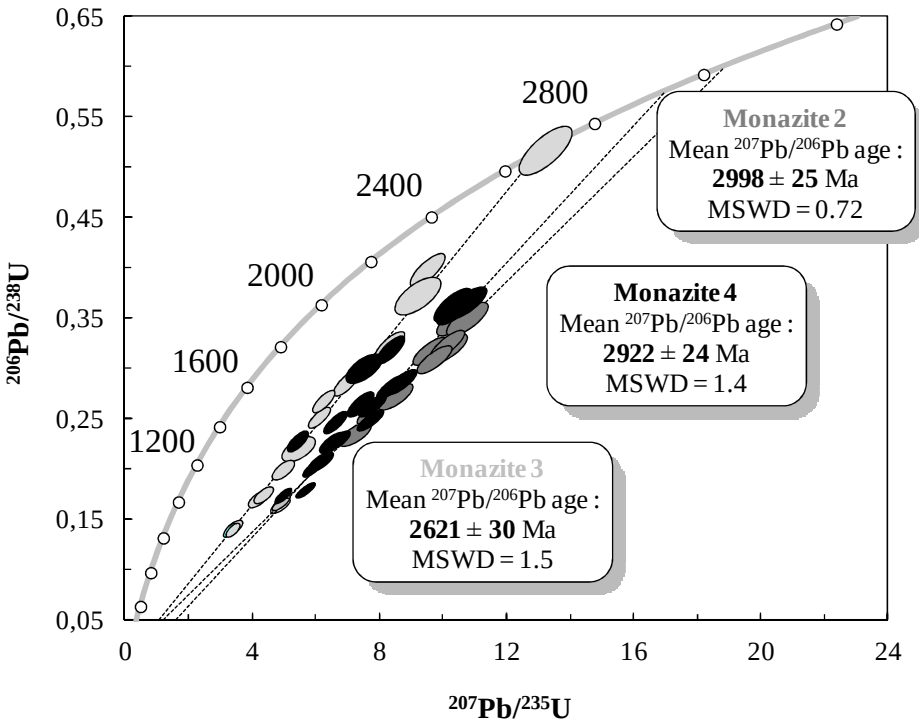

Figure 13

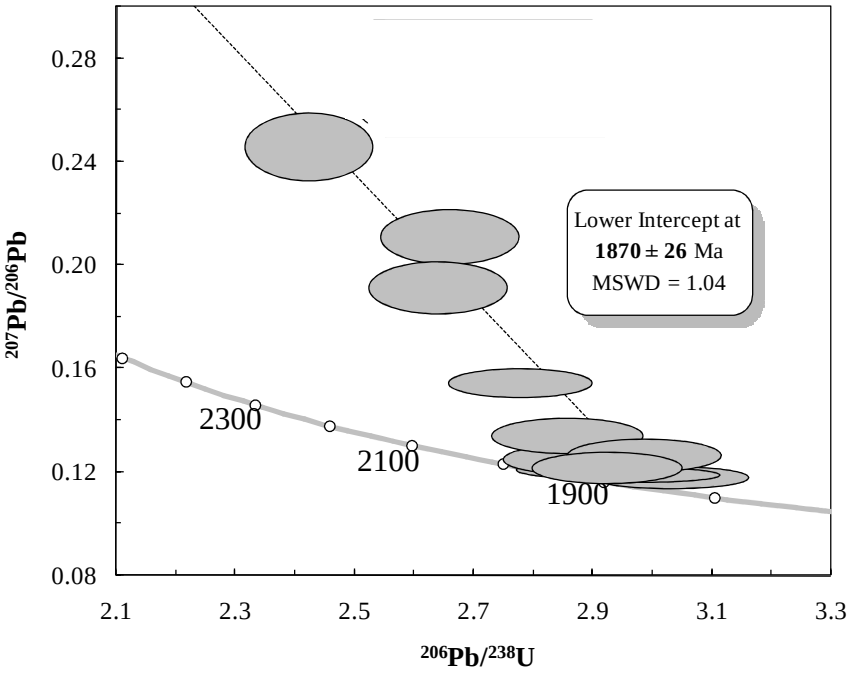

Figure 14

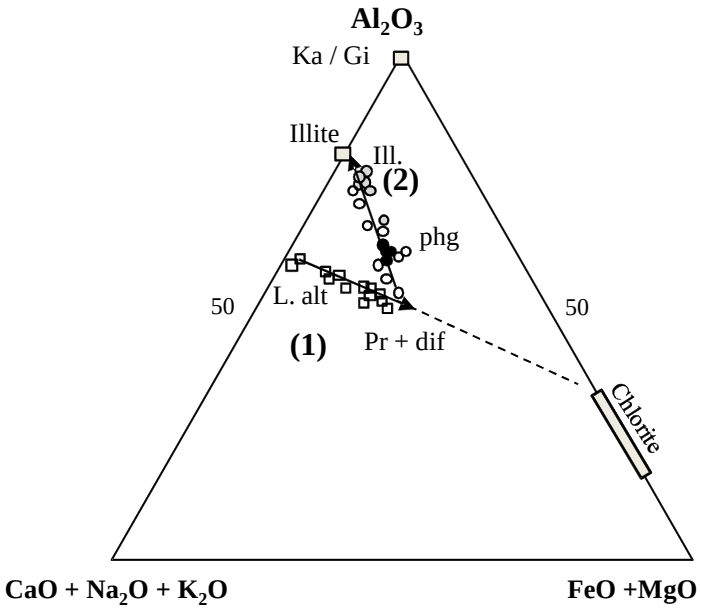

Figure 15

Table 1

	Granitoid					Sandstone	Granitoid						Sandstone
	GR23 640,50	GR23 631,50	GR23 630,90	GR23 629,90	GR23 629,25	GR23 629,18	GR20 851	GR20 845	GR20 833	GR20 825	GR20 821	GR20 819	GR20 818
SiO_2 (Wt%)	64,74	63,91	61,72	63,42	57,00	70,17	69,05	68,08	56,74	60,99	62,10	55,55	75,20
TiO_2	0,45	0,50	0,39	0,44	0,56	0,09	0,30	0,19	0,32	0,52	0,38	0,70	0,07
Al_2O_3	16,15	15,07	15,81	15,58	22,83	5,17	15,35	16,49	18,45	17,66	18,62	23,36	5,04
FeOt	4,23	4,01	3,93	4,07	4,08	0,87	2,65	1,86	8,16	4,71	4,33	6,86	0,62
MnO	0,05	0,06	0,07	0,02	0,02	0,00	0,03	0,02	0,06	0,07	0,04	0,01	0,00
MgO	3,15	2,05	1,88	1,22	1,46	0,31	1,79	0,89	1,61	2,06	2,01	0,73	0,26
CaO	2,24	4,19	5,07	2,67	0,58	8,17	2,03	3,07	6,68	5,32	1,12	0,69	6,50
Na_2O	5,13	4,66	5,49	2,42	0,35	0,07	5,21	5,84	4,66	5,46	2,30	0,14	0,03
K_2O	1,89	1,80	1,42	4,50	8,34	2,32	1,23	1,43	0,59	0,71	5,01	7,38	1,68
P_2O_3	0,23	0,26	0,23	0,27	0,03	0,00	0,10	0,08	0,07	0,14	0,08	0,19	0,04
LOI	1,95	3,53	4,17	4,52	4,03	12,20	1,65	1,55	2,09	2,03	3,26	3,94	9,10
Total	100,20	100,03	100,18	99,12	99,25	99,37	99,38	99,50	99,41	99,67	99,24	99,55	98,55
Ba (ppm)	1060,00	1147,00	476,40	4229,00	1700,00	830,40	401,20	622,10	243,70	388,30	2552,00	831,90	469,50
Rb	40,77	70,11	61,46	261,50	433,60	107,80	30,21	32,20	15,80	17,39	247,00	259,20	62,30
Sn	1,12	1,18	1,07	0,97	1,91	0,32	0,59	0,00	0,91	1,16	0,87	1,93	0,31
Sr	802,90	695,90	533,40	775,50	115,50	780,00	490,10	738,60	1293,00	573,20	204,50	15,23	385,50
Ga	21,62	21,71	20,30	20,46	33,50	6,43	17,50	17,85	26,20	22,31	23,63	29,91	6,09
Y	9,72	11,63	11,09	12,01	25,19	7,12	3,76	3,66	9,05	14,35	7,46	13,02	3,71
Zr	141,80	179,50	137,30	155,50	221,00	337,00	59,26	100,80	368,40	158,80	32,17	286,50	124,20
Nb	4,07	3,61	2,83	3,54	7,49	2,29	2,10	1,32	1,04	3,62	2,73	7,48	1,83
Cs	0,50	1,89	1,43	4,49	16,31	1,52	0,42	0,33	0,33	0,27	4,32	17,79	3,04
Cu	0,00	47,83	93,11	20,02	8,18	10,75	7,91	23,41	5,25	15,86	39,96	4,06	22,26
Zn	67,14	66,51	99,82	93,88	81,95	19,63	43,66	33,26	76,97	66,83	110,70	39,94	15,07
Hf	3,59	4,34	3,35	3,82	5,39	7,78	1,63	2,87	8,81	3,82	1,00	6,99	3,17
Ta	0,26	0,23	0,20	0,44	0,45	0,25	0,14	0,08	0,11	0,35	0,20	0,42	0,17
Pb	7,20	42,63	381,32	23,23	19,27	5,44	6,62	10,64	8,72	10,26	3,24	8,25	1,93
Th	5,68	7,55	2,20	41,43	12,45	11,86	2,85	0,62	7,52	1,16	4,56	20,04	6,45
U	0,50	1,05	1,31	4,33	4,78	3,59	0,57	0,52	2,50	0,34	0,95	5,69	1,22
V	64,36	74,24	70,28	62,46	256,10	146,40	40,54	14,51	80,11	73,27	51,95	84,92	19,92
La	33,46	65,07	58,12	39,61	114,90	14,42	11,47	12,42	22,37	11,01	17,16	20,31	3,40
Ce	59,83	119,40	105,20	75,67	180,30	24,56	22,37	25,32	41,44	25,44	29,71	41,50	5,93
Pr	6,76	12,87	11,33	9,08	19,94	3,15	2,71	3,01	4,23	3,42	3,42	4,77	0,75
Nd	24,99	46,31	41,11	32,99	74,04	12,13	10,30	11,32	13,56	14,44	2,73	17,84	2,85
Sm	4,28	7,29	6,41	5,78	12,69	2,40	1,72	1,92	2,00	3,18	2,85	2,94	0,60
Eu	1,36	1,68	1,35	1,87	2,98	0,66	0,56	0,53	0,61	0,73	0,90	0,64	0,21
Gd	3,02	4,46	3,94	4,15	9,36	1,84	1,23	1,11	1,61	2,77	2,15	2,62	0,70
Tb	0,37	0,52	0,48	0,54	1,21	0,24	0,16	0,14	0,22	0,43	0,30	0,37	0,10
Dy	1,80	2,44	2,25	2,65	5,90	1,19	0,75	0,66	1,24	2,57	1,64	2,14	0,63
Ho	0,31	0,39	0,37	0,42	0,89	0,22	0,13	0,12	0,26	0,49	0,29	0,45	0,12
Er	0,80	1,02	0,99	1,05	2,07	0,67	0,35	0,32	0,78	1,41	0,77	1,41	0,34
Tm	0,11	0,14	0,14	0,14	0,26	0,10	0,05	0,04	0,12	0,21	0,11	0,22	0,05
Yb	0,72	0,93	0,89	0,87	1,53	0,78	0,16	0,14	0,22	1,36	0,72	0,37	0,34
Lu	0,11	0,14	0,14	0,13	0,19	0,14	0,06	0,05	0,15	0,21	0,10	0,26	0,06

Table 1 (Continued)

	Granitoid					Sandstone	Granitoid										Sandstone
	GR31 873	GR31 866	GR31 863	GR31 859	GR31 858	GR31 857	KA6 472	KA6 467,90	KA6 462	KA6 454	KA6 449	KA6 445,60	KA6 444	KA6 438,7	KA6 437,85	KA6 437	KA6 432
SiO_2 (Wt %)	73,73	74,47	62,19	73,33	66,75	86,53	73,68	69,54	52,11	65,63	65,07	74,17	65,20	71,01	60,91	56,67	92,05
TiO_2	0,14	0,23	0,62	0,13	0,21	0,09	0,04	0,33	0,99	0,45	0,40	0,04	0,47	0,42	0,61	0,87	0,05
Al_2O_3	14,68	12,78	17,78	14,37	20,33	6,78	13,92	14,18	17,26	16,52	16,27	13,81	15,24	15,27	22,43	22,71	3,92
FeOt	1,76	2,80	5,46	2,39	1,44	0,70	0,30	3,32	9,41	4,03	4,86	0,47	4,58	2,40	2,76	6,20	0,20
MnO	0,02	0,02	0,10	0,01	0,03	0,01	0,01	0,03	0,09	0,03	0,04	0,01	0,05	0,02	0,01	0,03	0,00
MgO	0,38	0,43	2,38	0,74	0,59	0,27	0,17	1,45	3,50	1,47	1,59	0,16	1,82	0,66	0,91	1,67	0,10
CaO	1,14	1,21	0,75	0,32	0,16	0,44	0,89	1,27	4,26	1,59	1,61	1,47	1,53	1,75	0,42	0,06	0,04
Na_2O	4,85	4,27	3,61	1,93	0,09	0,05	4,03	5,81	4,43	5,59	5,53	4,61	5,18	5,00	0,07	0,09	0,12
K_2O	3,02	2,39	3,82	4,18	6,11	2,19	4,92	1,48	2,32	2,25	1,93	3,31	1,90	2,29	7,40	7,25	1,97
P_2O_3	0,03	0,08	0,19	0,03	0,03	0,06	0,00	0,19	0,82	0,23	0,23	0,00	0,21	0,22	0,28	0,03	0,00
LOI	0,76	0,95	2,82	1,72	3,52	1,77	0,99	1,42	4,26	1,78	2,12	1,36	2,64	1,67	3,90	3,89	0,51
Total	100,51	99,61	99,72	99,14	99,24	98,88	98,93	99,02	99,44	99,57	99,63	99,40	98,81	100,71	99,69	99,47	98,95
Ba (ppm)	1014,00	740,50	577,10	874,60	538,40	1800,00	3861,00	976,40	1355,00	2100,00	1551,00	5313,00	1109,00	990,40	2007,00	2237,00	543,70
Rb	61,78	60,31	194,40	182,50	168,60	74,69	95,06	25,94	70,29	62,86	54,99	59,19	63,20	71,04	246,80	252,40	59,84
Sn	0,62	0,72	1,54	0,58	0,75	0,00	0,00	1,05	2,07	1,20	1,33	0,00	3,23	0,89	3,45	1,89	0,00
Sr	222,40	202,30	121,80	59,10	15,89	131,80	553,80	658,20	643,50	659,70	587,60	634,60	370,10	586,30	57,23	52,65	32,24
Ga	17,28	17,18	24,91	20,08	26,15	8,77	13,20	16,31	24,81	22,77	23,01	14,97	23,95	18,14	31,57	28,22	4,31
Y	4,62	13,04	8,68	12,32	11,28	3,97	0,80	9,95	35,31	11,16	11,25	2,02	9,67	8,55	11,46	15,69	2,11
Zr	57,04	165,80	110,60	97,47	167,30	47,66	16,28	120,30	234,30	154,00	146,90	50,36	160,50	150,50	218,10	262,70	59,63
Nb	2,91	5,71	3,92	2,97	5,50	1,34	0,21	3,61	8,33	5,07	5,08	0,23	5,39	4,86	6,21	10,41	1,31
Cs	0,55	0,71	3,40	2,72	8,01	4,47	0,55	0,15	1,85	0,79	0,91	0,39	1,25	2,14	15,50	7,05	1,10
Cu	6,54	11,37	34,02	4,29	0,00	12,30	8,30	17,85	65,30	42,13	18,92	123,80	41,43	0,00	0,00	0,00	5,55
Zn	30,30	41,49	268,60	74,10	59,29	29,28	0,00	46,25	130,00	50,28	62,36	0,00	58,56	32,64	39,11	73,37	0,00
Hf	1,61	4,71	3,05	3,43	5,39	1,33	0,38	2,96	5,47	3,79	3,65	1,60	3,98	3,63	5,42	6,92	1,63
Ta	0,15	0,35	0,27	0,08	0,24	0,12	0,01	0,21	0,47	0,33	0,34	0,02	0,34	0,43	0,67	1,00	0,13
Pb	7,25	6,66	5,70	10,27	3,43	2,07	8,99	4,04	29,46	45,59	16,15	10,68	45,39	88,14	5,57	10,07	4,50
Th	1,38	8,79	2,09	4,37	9,97	4,13	0,77	15,08	17,55	10,46	6,38	0,67	12,69	8,79	7,52	24,00	3,45
U	0,51	0,89	1,49	1,99	2,78	1,35	0,23	2,78	4,98	3,97	2,78	0,61	3,97	4,83	2,83	12,94	0,60
V	10,49	18,94	79,74	67,65	14,88	14,27	4,92	86,66	199,90	116,20	128,40	4,08	88,59	37,92	54,50	75,21	2,50
La	6,82	11,55	14,41	25,61	4,92	17,36	1,45	34,16	103,70	67,71	49,74	10,40	45,73	25,89	55,00	11,44	11,30
Ce	12,31	23,10	28,22	46,72	10,56	28,32	2,25	63,12	213,90	124,50	103,90	17,91	88,34	50,81	101,30	22,80	16,67
Pr	1,26	2,72	3,44	5,22	1,17	3,49	0,23	7,55	24,13	14,27	11,01	1,85	9,58	5,97	10,45	2,88	1,99
Nd	2,91	5,71	3,92	2,97	4,60	11,81	0,85	27,66	96,64	51,54	40,18	6,34	5,39	22,82	45,21	12,33	6,61
Sm	0,94	2,21	2,96	3,66	1,33	2,07	0,17	4,79	16,82	7,69	6,53	0,85	6,65	3,99	8,11	3,55	0,90
Eu	0,61	0,76	0,89	0,95	0,45	0,52	0,21	3,15	11,24	4,50	3,93	0,56	1,21	2,83	1,57	1,33	0,21
Gd	0,91	2,30	2,69	2,92	1,56	1,65	0,15	0,41	1,42	0,49	0,47	0,06	4,01	0,34	5,05	3,41	0,55
Tb	0,15	0,38	0,35	0,41	0,25	0,20	0,02	2,10	7,20	2,27	2,32	0,32	0,46	1,70	0,58	0,50	0,07
Dy	0,83	2,24	1,78	2,23	1,62	0,86	0,11	2,10	7,20	2,27	2,32	0,32	2,14	1,70	2,67	2,73	0,38
Ho	0,15	0,43	0,27	0,40	0,35	0,13	0,02	0,35	1,25	0,37	0,39	0,06	0,34	0,29	0,43	0,48	0,06
Er	0,40	1,14	0,62	1,04	0,96	0,30	0,07	0,96	3,40	0,97	1,08	0,18	0,91	0,81	1,15	1,27	0,19
Tm	0,06	0,17	0,08	0,15	0,14	0,04	0,01	0,13	0,48	0,14	0,15	0,03	0,13	0,11	0,17	0,19	0,03
Yb	0,36	1,16	0,47	0,99	1,01	0,24	0,07	0,87	3,06	0,94	1,01	0,20	0,83	0,78	1,14	1,23	0,17
Lu	0,06	0,19	0,07	0,16	0,17	0,04	0,01	0,13	0,48	0,15	0,15	0,03	0,12	0,13	0,18	0,19	0,03

Table 2

	Chlorite in the propylitic zone								
SiO_2 (Wt %)	27,42	27,33	27,19	28,99	28,69	31,08	28,79	27,55	29,01
TiO_2	0,05	0,04	0,03	0,06	0,77	0,18	0,21	0,06	0,15
Al_2O_3	16,35	16,19	16,31	19,32	18,53	18,46	19,63	19,05	19,05
FeOt	18,48	14,92	13,89	22,73	21,88	19,65	22,95	25,72	25,95
MnO	0,20	0,16	0,20	0,65	0,40	0,12	0,74	0,35	0,20
MgO	19,94	20,13	19,78	17,21	17,27	18,71	17,33	15,54	14,55
CaO	0,09	0,12	0,02	0,03	0,29	0,07	0,05	0,06	0,03
Na_2O	0,09	0,04	0,02	0,03	0,03	0,05	0,00	0,02	0,02
K_2O	0,05	0,10	0,08	0,07	0,04	0,09	0,04	0,04	0,26
Total	82,66	79,01	77,50	89,07	87,92	88,40	89,74	88,39	89,22
Si	2,97	3,03	3,05	2,95	2,95	3,12	2,91	2,88	2,99
Al^{IV}	1,03	0,97	0,95	1,05	1,05	0,88	1,09	1,12	1,01
Al^{VI}	1,05	1,14	1,21	1,27	1,20	1,30	1,26	1,23	1,31
Ti	0,00	0,00	0,00	0,00	0,06	0,01	0,02	0,00	0,01
Fe^{2+}	1,67	1,38	1,30	1,94	1,88	1,65	1,94	2,25	2,24
Mg	3,22	3,32	3,31	2,61	2,65	2,80	2,61	2,42	2,24
Mn	0,02	0,01	0,02	0,06	0,04	0,01	0,06	0,03	0,02
Ca	0,01	0,01	0,00	0,00	0,03	0,01	0,01	0,01	0,00
Na	0,02	0,01	0,00	0,01	0,01	0,01	0,00	0,00	0,00
K	0,01	0,01	0,01	0,01	0,01	0,01	0,01	0,01	0,03
∑ oct	5,94	5,84	5,83	5,82	5,73	5,74	5,81	5,90	5,79
Fe/(Fe+Mg)	0,34	0,29	0,28	0,43	0,42	0,37	0,43	0,48	0,50

Table 3

	Chlorite in the illitic zone						
SiO_2 (Wt %)	27,65	26,27	26,40	26,18	25,47	26,38	27,97
TiO_2	2,05	2,10	1,83	1,35	0,03	0,04	0,19
Al_2O_3	15,62	15,58	15,85	15,51	17,79	18,77	21,39
FeOt	31,22	31,48	29,90	32,43	31,55	29,70	34,02
MnO	0,34	0,21	0,46	0,40	0,42	0,37	0,16
MgO	10,27	10,70	10,44	10,18	10,57	10,79	5,82
CaO	0,08	0,07	0,09	0,13	0,06	0,03	0,02
Na_2O	0,05	0,02	0,07	0,04	0,06	0,01	0,00
K_2O	0,20	0,13	0,15	0,44	0,33	0,64	0,91
Total	87,48	86,55	85,18	86,65	86,29	86,73	90,47
Si	3,02	2,92	2,96	2,93	2,85	2,89	2,87
Al^{IV}	0,98	1,08	1,04	1,07	1,15	1,11	1,13
Al^{VI}	1,04	0,96	1,05	0,98	1,19	1,32	1,47
Ti	0,17	0,18	0,15	0,11	0,00	0,00	0,02
Fe^{2+}	2,86	2,93	2,80	3,04	2,95	2,72	3,22
Mg	1,67	1,77	1,74	1,70	1,76	1,76	1,03
Mn	0,03	0,02	0,04	0,04	0,04	0,03	0,03
Ca	0,01	0,01	0,01	0,01	0,01	0,00	0,00
Na	0,01	0,00	0,02	0,01	0,01	0,00	0,06
K	0,03	0,02	0,02	0,06	0,05	0,09	0,06
∑ oct	5,57	5,66	5,60	5,72	5,90	5,80	5,72
Fe/(Fe+Mg)	0,63	0,62	0,62	0,64	0,63	0,61	0,76

Table 4

	Phengite								
SiO_2 (Wt %)	48,54	46,16	46,05	47,05	50,79	46,02	47,94	47,29	47,42
TiO_2	0,09	0,09	0,12	0,15	0,08	0,10	0,02	0,10	0,13
Al_2O_3	26,03	26,84	26,90	25,19	27,04	26,45	28,16	26,72	27,89
FeOt	5,09	5,72	5,43	5,14	4,38	5,99	4,45	5,03	4,67
MnO	0,03	0,08	0,03	0,03	0,12	0,12	0,01	0,05	0,02
MgO	2,07	2,09	1,94	1,79	2,62	1,89	1,97	2,01	1,91
CaO	0,05	0,02	0,09	0,12	0,15	0,04	0,04	0,00	0,05
Na_2O	0,06	0,03	0,08	0,25	0,07	0,12	0,09	0,03	0,09
K_2O	10,15	10,14	9,90	9,46	9,91	10,24	10,60	10,57	10,78
Total	92,10	91,17	90,54	89,16	95,15	90,97	93,29	91,79	92,96
Si	3,36	3,25	3,26	3,36	3,38	3,26	3,28	3,30	3,27
Al^{IV}	0,64	0,75	0,74	0,64	0,62	0,74	0,72	0,70	0,73
Al^{VI}	1,49	1,48	1,50	1,49	1,51	1,47	1,55	1,50	1,54
Ti	0,00	0,00	0,01	0,01	0,00	0,01	0,00	0,01	0,01
Fe^{2+}	0,27	0,30	0,29	0,28	0,22	0,32	0,23	0,26	0,24
Mg	0,21	0,22	0,20	0,19	0,26	0,20	0,20	0,21	0,20
Mn	0,00	0,00	0,00	0,00	0,01	0,01	0,00	0,00	0,00
Ca	0,00	0,00	0,01	0,01	0,01	0,00	0,00	0,00	0,00
Na	0,01	0,00	0,01	0,03	0,01	0,02	0,01	0,00	0,01
K	0,90	0,91	0,89	0,86	0,84	0,92	0,93	0,94	0,95
Inter Charg	0,91	0,92	0,91	0,91	0,86	0,94	0,94	0,95	0,96
∑oct	1,97	2,00	2,00	1,95	1,99	1,99	1,99	1,98	1,98
Fe/(Fe+Mg)	0,55	0,58	0,59	0,59	0,46	0,61	0,53	0,56	0,55

Table 5

	Illite							
SiO_2 (Wt %)	53,18	48,09	52,96	48,03	47,47	52,21	53,30	48,89
TiO_2	0,29	0,08	0,09	0,05	0,01	0,09	0,11	0,14
Al_2O_3	35,37	34,46	36,45	34,06	32,50	36,27	36,23	32,59
Fe2O3	2,73	1,07	1,81	1,29	1,91	1,83	1,81	1,09
MnO	0,04	0,01	0,00	0,00	0,00	0,04	0,04	0,00
MgO	1,02	0,66	0,69	0,83	0,52	0,55	0,83	1,49
CaO	0,03	0,05	0,04	0,06	0,18	0,04	0,03	0,08
Na_2O	0,08	0,14	0,08	0,12	0,07	0,08	0,07	0,11
K_2O	9,51	9,54	9,37	9,81	8,74	9,45	9,40	9,94
Total	102,25	94,08	101,48	94,25	91,40	100,55	101,81	94,32
Si	3,25	3,19	3,24	3,19	3,24	3,23	3,25	3,25
Al_{IV}	0,75	0,81	0,76	0,81	0,76	0,77	0,75	0,75
Al^{VI}	1,79	1,89	1,87	1,86	1,85	1,88	1,86	1,80
Ti	0,01	0,00	0,00	0,00	0,00	0,00	0,01	0,01
Fe^{2+}	0,13	0,05	0,08	0,06	0,10	0,09	0,08	0,05
Mg	0,09	0,06	0,06	0,08	0,05	0,05	0,08	0,15
Mn	0,00	0,00	0,00	0,00	0,00	0,00	0,00	0,00
Ca	0,00	0,00	0,00	0,00	0,01	0,00	0,00	0,01
Na	0,01	0,02	0,01	0,01	0,01	0,01	0,01	0,01
K	0,74	0,81	0,73	0,83	0,76	0,75	0,73	0,84
Inter Charg	0,75	0,83	0,74	0,84	0,78	0,76	0,74	0,86
$\sum$ oct	2,01	2,01	2,02	2,01	2,00	2,01	2,02	2,00
Fe/(Fe+Mg)	0,58	0,65	0,57	0,59	0,76	0,63	0,52	0,58

Table 6

	Epidote					Allanite							
Na_2O (Wt %)	0,10	0,15	0,10	0,04	0,00	0,06	0,04	0,10	0,04	0,03	0,02	0,08	0,04
MgO	0,00	0,01	0,11	0,01	0,18	0,22	0,16	0,12	0,44	0,28	0,80	0,12	0,25
Al_2O_3	19,84	21,31	19,26	21,06	22,08	13,59	13,69	13,65	13,19	14,56	17,23	15,82	18,27
SiO_2	34,15	36,96	32,96	35,67	37,94	28,98	30,00	29,06	28,79	28,03	32,56	28,11	33,05
K_2O	0,05	0,11	0,03	0,04	0,01	0,08	0,04	0,06	0,10	0,03	0,03	0,06	0,03
CaO	20,28	21,00	20,58	21,65	21,46	10,15	10,74	10,64	12,00	10,45	11,03	11,11	11,30
TiO_2	0,11	0,07	0,04	0,04	0,45	0,23	0,44	0,47	1,70	0,22	0,64	0,24	0,13
MnO	0,00	0,06	0,02	0,12	14,74	0,20	0,33	0,13	0,14	0,22	0,24	0,48	0,62
FeOt	14,34	14,39	14,68	14,23	0,01	15,25	15,48	14,41	14,45	12,26	12,40	10,76	12,01
Nd_2O_3	0,00	0,00	0,16	0,00	0,36	3,07	1,79	1,03	1,34	3,15	3,25	1,48	2,83
Ce_2O_3	0,32	0,15	0,20	0,90	0,00	10,11	9,82	9,55	9,87	10,91	10,37	9,84	9,23
La_2O_3	0,38	0,13	0,27	0,00	0,09	6,67	6,04	5,80	4,41	5,92	5,70	5,52	5,40
Total	89,57	94,33	88,42	93,76	97,32	88,61	88,56	85,03	86,46	86,06	94,26	83,64	93,16
Si	2,99	3,05	2,95	2,99	3,03	2,95	3,00	3,01	2,94	2,93	3,01	2,95	3,05
Al	2,05	2,07	2,03	2,08	2,08	1,63	1,62	1,67	1,59	1,79	1,88	1,96	1,99
Ti	0,01	0,00	0,00	0,00	0,03	0,02	0,03	0,04	0,13	0,02	0,04	0,02	0,01
Mn	0,00	0,00	0,00	0,01	0,00	0,02	0,03	0,01	0,01	0,02	0,02	0,04	0,05
Fe^{2+}	0,94	0,89	0,99	0,90	0,89	1,17	1,17	1,12	1,11	0,97	0,86	0,85	0,83
Mg	0,00	0,00	0,01	0,00	0,02	0,03	0,02	0,02	0,07	0,04	0,11	0,02	0,03
Ca	1,90	1,86	1,98	1,94	1,84	1,11	1,15	1,18	1,31	1,17	1,09	1,25	1,12
Na	0,02	0,02	0,02	0,01	0,00	0,01	0,01	0,02	0,01	0,01	0,00	0,02	0,01
K	0,01	0,01	0,00	0,00	0,00	0,01	0,00	0,01	0,01	0,00	0,00	0,01	0,00
Nd	0,00	0,00	0,01	0,00	0,01	0,16	0,09	0,06	0,07	0,17	0,15	0,08	0,13
Ce	0,01	0,00	0,01	0,03	0,00	0,38	0,36	0,36	0,37	0,42	0,35	0,38	0,31
La	0,01	0,00	0,01	0,00	0,00	0,25	0,22	0,22	0,17	0,23	0,19	0,21	0,18
Fe/(Fe+Al)	0,32	0,30	0,33	0,30	0,30	0,42	0,42	0,40	0,41	0,35	0,31	0,30	0,30

Table 7

	Monazite (KA6 437,85)				Monazite (GR1 631)			
SiO_2 (Wt %)	0,37	1,22	0,39	0,43	0,88	0,22	0,72	0,42
P_2O_5	30,73	29,76	30,99	30,76	30,13	28,66	29,55	29,66
CaO	1,14	1,37	1,12	1,18	0,28	0,25	0,28	0,20
Y_2O_3	0,97	0,90	0,99	1,04	0,74	0,79	0,68	0,59
La_2O_3	15,05	14,98	15,61	15,63	18,74	18,17	17,30	20,10
Ce_2O_3	30,47	29,80	30,31	30,07	33,50	33,26	33,76	33,16
Pr_2O_3	2,99	2,92	2,95	3,04	3,54	3,88	3,33	3,21
Nd_2O_3	13,10	11,93	12,42	12,01	8,20	8,76	8,30	7,32
Sm_2O_3	1,40	1,65	1,51	1,65	0,59	0,67	0,37	0,59
Gd_2O_3	0,72	0,69	0,63	0,79	0,37	0,79	0,47	0,08
PbO	0,05	0,13	0,08	0,09	0,02	0,02	0,04	0,00
ThO_2	0,87	1,33	0,72	0,96	0,03	0,00	0,01	0,01
UO_2	0,01	0,01	0,00	0,02	0,01	0,09	0,04	0,01
Total	97,46	96,27	97,29	97,22	97,04	95,57	94,85	95,36
Th/La	0,06	0,09	0,05	0,06	0,00	0,00	0,00	0,00
ΣREE	64,71	62,86	64,42	64,23	65,68	66,32	64,20	65,07

Table 8

					2 sigma error		2 sigma error		Age (Ma)	2 sigma error
Pb ppm	Th ppm	U ppm	Th/U	Pb207/U235	Pb207/U235	Pb206/U238	Pb206/U238	Rho	Pb207/Pb206	Pb207/Pb206
473	5291	42	125	10,43	0,51	0,35	0,01	0,76	2949	76
525	6228	56	112	7,68	0,33	0,26	0,01	0,82	2956	64
370	4400	34	131	10,04	0,56	0,32	0,01	0,72	3031	89
341	3703	29	126	10,77	0,55	0,35	0,01	0,75	3001	79
415	4816	45	107	9,56	0,46	0,31	0,01	0,77	2997	74
580	6964	60	116	10,14	0,45	0,33	0,01	0,81	3026	67
507	5934	59	100	8,48	0,44	0,27	0,01	0,74	3016	82
316	2877	32	89	9,73	0,45	0,31	0,01	0,79	3032	71
384	4442	48	92	7,21	0,41	0,24	0,01	0,70	2993	91
			-					-		-
558	7279	65	112	5,43	0,44	0,22	0,01	0,58	2640	138
786	10178	125	82	3,43	0,21	0,14	0,01	0,65	2598	102
861	10420	84	124	6,10	0,28	0,25	0,01	0,77	2610	73
680	7568	60	126	6,95	0,33	0,29	0,01	0,76	2618	75
740	8807	81	109	6,24	0,28	0,27	0,01	0,77	2542	72
303	3611	50	72	4,15	0,25	0,17	0,01	0,65	2622	100
509	7707	138	56	3,29	0,17	0,14	0,01	0,72	2559	82
273	3438	42	81	4,97	0,30	0,20	0,01	0,66	2658	99
296	3850	66	59	4,34	0,24	0,18	0,01	0,68	2648	92
345	4850	82	59	3,37	0,19	0,14	0,01	0,67	2599	93
676	7159	61	118	9,49	0,44	0,40	0,01	0,78	2584	72
391	3131	23	136	13,20	0,68	0,52	0,02	0,73	2698	82
283	1741	24	72	9,19	0,58	0,37	0,02	0,65	2642	104
798	9406	68	139	8,30	0,37	0,32	0,01	0,80	2705	68
748	11219	117	96	5,68	0,24	0,18	0,01	0,83	3049	63
738	11372	122	93	4,90	0,23	0,17	0,01	0,77	2924	74
735	10807	118	91	4,97	0,22	0,17	0,01	0,80	2878	67
780	11614	99	117	5,89	0,26	0,20	0,01	0,80	2916	67
669	8923	63	142	8,68	0,39	0,29	0,01	0,80	2975	67
631	8724	66	132	7,70	0,33	0,25	0,01	0,81	3009	65
631	8254	56	146	7,38	0,36	0,27	0,01	0,75	2841	77
736	9649	62	157	7,75	0,35	0,26	0,01	0,79	2930	69
597	7892	52	152	6,15	0,31	0,21	0,01	0,74	2942	80
490	6660	56	119	4,86	0,26	0,16	0,01	0,72	2936	84
707	9391	60	156	6,69	0,31	0,23	0,01	0,78	2920	71
754	10964	88	125	6,61	0,30	0,25	0,01	0,79	2780	69
680	9151	81	114	5,40	0,26	0,23	0,01	0,73	2576	78
736	9140	61	151	8,32	0,38	0,32	0,01	0,78	2733	71
622	7734	60	128	6,51	0,32	0,23	0,01	0,74	2891	78
450	5431	38	145	10,28	0,49	0,36	0,01	0,76	2865	73
555	6692	50	135	10,38	0,48	0,36	0,01	0,77	2912	72
606	7235	40	180	10,74	0,52	0,37	0,01	0,76	2927	75
556	6780	64	106	8,36	0,37	0,28	0,01	0,79	2941	67
352	2909	36	81	7,49	0,46	0,30	0,01	0,65	2658	101

Table 9

GR1-631 Analysis_	Pb ppm	Th ppm	U ppm	Th/U	Pb207/U235	2 sigma error Pb207/U235	Pb206/U238	2 sigma error Pb206/U238	Rho	Age (Ma) Pb207/Pb206	2 sigma error Pb207/Pb206
05120912c	231	1429	337	4,2	5,78	0,24	0,35	0,01	0,85	1976	63
06120912c	143	582	316	1,8	5,38	0,24	0,33	0,01	0,78	1931	73
07120912c	265	1799	399	4,5	5,51	0,22	0,33	0,01	0,87	1948	60
08120912c	191	1387	199	7,0	7,69	0,35	0,36	0,01	0,78	2401	70
17120912c	72	31	224	0,1	6,03	0,31	0,35	0,01	0,68	2037	86
18120912c	125	442	264	1,7	6,49	0,36	0,35	0,01	0,65	2157	92
19120912c	96	77	303	0,3	5,87	0,32	0,34	0,01	0,66	2057	90
20120912c	158	234	466	0,5	5,78	0,31	0,34	0,01	0,66	1993	90
21120912c	133	25	301	0,1	10,97	0,60	0,38	0,01	0,66	2917	84
22120912c	322	2263	294	7,7	10,03	0,56	0,38	0,01	0,64	2760	88
23120912c	363	1934	359	5,4	14,02	0,79	0,41	0,01	0,64	3161	86

Table 10

Sample	$\delta^{18}O$ (‰ SMOW)	$\delta^{13}C$ (‰ PDB)
GR5-510	11,5	-5,33
GR23-630,9	10,5	-13,76
GR23-631,5	10,9	-9,56
GR43-636	10,4	-7,02
GR43-638	10,2	-6,80
KA6-462	17,7	-10,65